Physics of Fluids

RESEARCH ARTICLE | JANUARY 19 2024

Lagrangian investigation of the correlation of helicity with coherent flow characteristics for turbulent transport

Oanh L. Pham ; Dimitrios V. Papavassiliou

Physics of Fluids 36, 015133 (2024)
https://doi.org/10.1063/5.0180949

Physics of Fluids ARTICLE pubs.aip.org/aip/pof

Lagrangian investigation of the correlation of helicity with coherent flow characteristics for turbulent transport

Cite as: Phys. Fluids **36**, 015133 (2024); doi: 10.1063/5.0180949
Submitted: 13 October 2023 · Accepted: 22 December 2023 ·
Published Online: 19 January 2024

Oanh L. Pham and Dimitrios V. Papavassiliou[a)]

AFFILIATIONS

School of Sustainable Chemical, Biological and Materials Engineering, The University of Oklahoma, 100 East Boyd St., SEC T-335, Norman, Oklahoma 73019, USA

[a)]**Author to whom correspondence should be addressed:** dvpapava@ou.edu. **Tel.:** (405) 325-5811

ABSTRACT

The correlation between helicity and turbulent transport in turbulent flows is probed with the use of direct numerical simulation and Lagrangian scalar tracking. Channel flow and plane Couette flow at friction Reynolds number 300 and Lagrangian data along the trajectories of fluid particles and passive particles with Schmidt numbers 0.7 and 6 are used. The goal is to identify characteristics of the flow that enhance turbulent transport from the wall, and how flow regions that exhibit these characteristics are related to helicity. The relationship between vorticity and relative helicity along particle trajectories is probed, and the relationship between the distribution of helicity conditioned on Reynolds stress quadrants is also evaluated. More importantly, the correlation between relative helicity density and the alignment of vorticity with velocity vectors and eigenvectors of the rate of strain tensor is presented. Separate computations for particles that disperse the farthest into the flow field and those that disperse the least are conducted to determine the flow structures that contribute to turbulent dispersion. The joint distribution of helicity and vertical velocity, and helicity and vertical vorticity depends on the location of particle release and the Schmidt number. The trajectories of particles that disperse the least are characterized by a correlation between the absolute value of the relative helicity density and the absolute value of the cosine between the vorticity vector and the eigenvectors of the rate of strain tensor, while the value of this correlation approaches zero for the particles that disperse the most.

I. INTRODUCTION

Helicity is one of the features of turbulent flows whose role in sustaining turbulence and in enhancing turbulent transport needs clarification.[1,2] It is defined as the volume integral of the scalar product of velocity $\boldsymbol{u}$ and vorticity $\boldsymbol{\omega}$, and helicity density is defined as $H = \boldsymbol{u} \cdot \boldsymbol{\omega}$.[3] The sign of helicity depends on whether right-handed or left-handed helical motions are dominant in the flow. Helicity is a topological quantity that describes the degree to which vortex lines of the flow are tangled and intertwined and it may be present in laminar as well as in turbulent flow.[4,5] Helicity and kinetic energy are two inviscid quadratic invariants in 3D turbulent flows.[6–8] Helicity is associated with the corkscrew motion of the fluid and it can be found in tornadoes, hurricanes, and in rotating thunderstorms in the atmosphere and in Langmuir circulations in the oceans. More importantly, helicity could indicate reduced aerodynamic drag and improved mixing effectiveness of reactants.[9,10] Helicity is not only important in atmospheric and geophysical flows but also in biomedical research to quantify swirling motions in cardiovascular flows.[11] It is also a crucial and universal property of 3D coherent structures in turbulence and transitional flows,[12–15] and it has been argued that the existence of mean helicity in turbulent flows could enhance transport.[16]

Prior studies have focused on the use of helicity spectra to investigate the role of helicity on the evolution of isotropic turbulent flow[17,18] and in turbulent channel flows with streamwise rotation.[19] The dynamics of helicity cascade from large to smaller scales of turbulence has also been investigated.[3,6,8,9,20] Other works have explored the effect of kinetic helicity (velocity–vorticity correlation) on momentum transport and the generation of large-scale flow,[21] the Reynolds stress budget in relation to the mean and fluctuating helicity budgets in channel flows,[22] the importance of helicity in rotating turbulence,[23] the geometrical and vortical statistics in small scales,[24] the helicity fluctuations in homogeneous isotropic turbulence,[13,15] and the relationship between helical flow structures and atherogenesis in coronary bypass models.[25]

The term coherent structures in turbulent flows refers to the spatiotemporal self-organization of the flow, and these structures have been associated with the production of turbulent kinetic energy and the sustainment of turbulence.[26–28] In the rotational form of the Navier–Stokes momentum equation, when the magnitude of the term $\boldsymbol{u} \times \boldsymbol{\omega}$ is small, the energy transfer is small. The minimization of this term occurs by the alignment of the two vectors, which is represented by helicity density, H. Therefore, the helicity density is important in evaluating coherent structures and their role in turbulence.[21,29] It has been argued that coherent structures are associated with flow regions in which helicity is large and turbulent kinetic energy dissipation is low. Low dissipation means that these coherent structures could survive for a long time in the flow and thus, helical structures could sustain coherent structures for long times.[30] Zhang *et al.* concluded that helicity can be used as an indicator for vortices—they found that the maximum normalized helicity density could be used to identify the vortex core and the sign of the normalized helicity density can be used to identify the swirling direction of a vortex.[31]

When studying experiments on helicity density of turbulent flow for a mixing layer, Wallace *et al.*[32] suggested that the streamwise vortices have significant relative helicity density (note that the relative helicity density is the normalized helicity density, i.e., the cosine between the velocity and vorticity vectors). However, their results did not clarify whether the relative helicity density should be large within coherent structures.[32] There have been other studies that employed experimental and computational methods to characterize the relationship of helicity and coherent structures. For example, Tsinober and Levich indicated that the 3D coherent structures in turbulence possess coherent helicity, but their experiments were carried out for transitional or rather low Reynolds number flows.[33] Tsinober and Levich explored the case of homogeneous turbulence and pointed out that the existence of helical structures and fluctuations in 3D turbulent flow are correlated with the phenomena of intermittency and coherent structures.[34] Pelz used direct numerical simulation (DNS) to suggest that the coherent structures, small-scale intermittency and helicity fluctuations are correlated.[35] Shtilman *et al.* used DNS of the Taylor–Green vortex and pointed out that in regions of small dissipation, the magnitude of relative helicity density is large and vorticity and curl of vorticity is nearly orthogonal.[36] DNS of unforced turbulence by Shtilman *et al.* showed spontaneous generation of helicity and helicity fluctuation, which revealed changes in the topological structure of the vorticity field.[29]

However, when investigating helicity in homogeneous turbulence, homogeneous irrotationally strained flows and homogeneous shear flows, and fully developed turbulent channel flow, Roger *et al.* showed no apparent correlation of the fluctuating helicity density with the well-known hairpin vortices or with strong spanwise coherent vortices.[30] The simulations showed that there was no evidence for the association of relative helicity with low dissipation or coherent structures.[30] Speziale suggested that it is unlikely that these helicity fluctuations can be correlated with turbulence activity such as coherent structures and small-scale intermittency because of the nature of the velocity and pressure field fluctuations.[37]

DNS and Lagrangian scalar tracking (LST) have been combined recently to examine the relationship between turbulent kinetic energy dissipation rate and helicity density along the trajectories of dispersing particles.[2,38] It was found that there is an effect of helicity on turbulent transport, but not because of an association of helical flow structures to low turbulent kinetic energy dissipation.[2] In fact, low turbulent dispersion was associated with a helicity-dissipation anticorrelation. However, it was apparent that the relationship between helicity and turbulent scalar transport needs further evaluation.

In this study, we continue to probe the role of helicity in turbulent transport by combining DNS and LST to compute the helicity at the location of passive particles that disperse at various Schmidt numbers, *Sc*. Since Lagrangian measurements in laboratory experiments are not trivial, especially when one wants to calculate derivatives of fluctuating velocity fields and simultaneously measure such quantities in three dimensions, we used computations to obtain such measurements along particle trajectories. In addition, LST is not limited to low Schmidt number fluidss.[39] The turbulent flow fields computed were for plane Poiseuille and plane Couette flow. This choice was made in order to provide insights into turbulent transport in relation to coherent flow structures. The turbulence structure of channel and Couette flows is different, since there is no turbulent kinetic energy production in the center of Poiseuille flow, while there is production in the center of a plane Couette flow channel. At the same time, the Reynolds stress in the center of a Poiseuille flow channel is zero, while it is finite for Couette flow.[40] The contributions of this paper are to (i) characterize the correlation between helicity and coherent structures by examining the vorticity, the vertical velocity, the distribution of helicity conditioned on the Reynolds stress quadrant events, and the *Q*-criterion; (ii) examine the effects of helicity on turbulent dispersion to assess the role of helicity in transport and its relevance to the coherent structures; (iii) investigate the correlation between normalized fluctuating helicity and the alignment of vorticity with the eigenvectors of the rate of strain tensors; and (iv) examine the effects of molecular dispersion, as expressed through the *Sc*, on all the above.

II. METHODS

A. Direct numerical simulation

The pseudospectral DNS algorithm of Lyons *et al.*[41,42] validated by the experiments of Günther *et al.*[43] was applied to simulate turbulent channel flow. This algorithm has been modified and used to simulate plane Couette flow.[39–42] Periodic boundary conditions were applied in the streamwise and spanwise directions of the flow field. The boundary conditions enforced at the channel walls were the no-slip and no-penetration conditions.[41] The Navier–Stokes equations in rotational form were expanded in terms of Fourier series in the streamwise and spanwise directions and in terms of Chebyshev polynomial series in the direction vertical to the channel walls. The velocity field was calculated through three fractional time steps. The first fractional step accounted for the nonlinear convective term and the mean pressure gradient. The second fractional step accounted for the dynamic pressure head term and the third fractional step accounted for the viscous term of the Navier–Stokes equation written in its rotational form.[44] The friction velocity, $u^* = (\tau_w/\rho)^{1/2}$, where τ_w is the wall shear stress and ρ is the fluid density, and the fluid kinematic viscosity, ν, were used to define the friction length scale and the friction timescale, so that all quantities were scaled in viscous wall units. From this point and on, all quantities presented are dimensionless using the viscous wall parameters, unless otherwise mentioned. The dimensions of the computational box were $16\,\pi h \times 2h \times 2\pi h$ for Poiseuille flow and $16\,\pi h \times 2h \times 2\pi h$ for Couette flow in the streamwise x, normal y, and spanwise z directions, respectively. The half channel height was

$h = 300$, so that the friction Reynolds number was also $Re_\tau = h = 300$. The number of grid points was $1024 \times 128 \times 256$ for Poiseuille and $1024 \times 256 \times 256$ for Couette flow in the streamwise x, normal y, and spanwise z directions.

Specifically for Couette flow, the walls of the channel moved in opposite directions relative to each other, while there was no mean pressure gradient. Therefore, in Couette flow, the code was modified by changing the Dirichlet boundary conditions at the walls, so that the streamwise velocity at the wall U_w was $U_w = \pm Gh$ and G was constant ($G = 0.064$).[2] The top wall of the channel moved in the negative x direction and the bottom wall moved in the positive x direction. Figure 1 is a depiction of the flow configuration. The Reynolds number defined for Poiseuille flow based on the mean centerline velocity, U_c, and the half channel height, $Re = (U_c h/\nu)$ and defined for Couette flow as $Re = (U_w h/\nu)$, was 5700. The fluid was assumed to be an incompressible Newtonian fluid. The time step for the simulation for Poiseuille flow was $\Delta t = 0.1$, and for Couette flow it was $\Delta t = 0.05$ in viscous wall time units.

B. Lagrangian scalar tracking

The behavior of dispersing scalar quantities was investigated by following the paths of many scalar markers in the flow field created by the DNS. Assuming that the fluid velocity was the same as the Lagrangian velocity $\boldsymbol{V}$ at the position of each scalar marker, the convective part of the marker motion was found by time integration. The convective part of the particle motion was calculated based on the following equation:[45]

$$\boldsymbol{V}(\boldsymbol{x}_0, t) = \frac{\partial \boldsymbol{X}(\boldsymbol{x}_0, t)}{\partial t}, \tag{1}$$

where the Lagrangian velocity of a marker released at location $\boldsymbol{x}_0$ is given as $\boldsymbol{V}(\boldsymbol{x}_0, t) = \boldsymbol{U}[\boldsymbol{X}(\boldsymbol{x}_0, t), t]$ and $\boldsymbol{U}$ is the Eulerian velocity of the fluid at the location of the marker at time t.[45–50] An Adams–Bashforth scheme was employed to integrate the equation of particle motion, and the velocity vector between grid points was estimated using a mixed sixth order Lagrangian–Chebyshev interpolation scheme.[51] At the end of each convection step, a random jump was imposed to compute the Brownian motion effects. The values of the random jump were taken from a normal probability density function (PDF) with a zero mean and a standard deviation that depended on the fluid properties and the molecular diffusivity of the particles. Einstein's theory for Brownian motion provided the relation between the rate of molecular dispersion and molecular diffusivity in each space direction as follows:[45–50]

$$\frac{d\overline{X^2}}{dt} = 2D, \tag{2}$$

where $\overline{X^2}$ is the mean-squared displacement in one space direction and D is the molecular diffusivity. Thus, a 3D random walk was added on the particle motion after each convective time step, taken from a normal distribution with a standard deviation $\sigma = \sqrt{2\Delta t/Sc}$ in viscous wall units. From this point on, in this manuscript, we will use mass transfer terminology and the Sc, even though all results are applicable for heat transfer expressed by the Prandtl number, Pr, of the dispersing scalar markers. The markers were assumed to be passive and had no effect on the flow.[46,52–54]

Note that while the trajectories of the $Sc = 0.7$ and 6 markers include a Brownian motion, the fluid particles do not. This allows a comparison between three cases: (a) molecular diffusion effects are important (i.e., $Sc = 0.7$); (b) convection is the only transport mechanism without any molecular diffusion (i.e., fluid particles); and (c) A situation between the two ($Sc = 6$). In this way, we can distinguish between the transport of a scalar vs a pure Lagrangian flow tracer and can explore the possibility that different flow structures contribute to transport in different ways when scalar quantities with different diffusivity are transported.

The markers were released into the flow after the Poiseuille and Couette flow reached stationary state. The Lagrangian simulations were carried out for fluid particles and for different Sc numbers, $Sc = 0.7$ and 6. The passive particles (i.e., markers whose presence does not affect the flow) were released at given distances Y_0 from the bottom wall of the computational channel, $Y_0 = 0$, 1.5, 3, 5, 10, 15, 75, and 300 for both Poiseuille and Couette flows. These release positions represented the channel wall, the viscous wall sublayer, the buffer region, the logarithmic layer, and the outer flow at the channel center. At each Y_0, 100 000 particles were evenly released from 20 lines that were spaced uniformly in the x direction and spanned the width of the channel in the z direction. Selecting different release points at the same xz plane avoided potential bias caused by the instantaneous initial velocity field. Therefore, the total number of particles was 800 000 for either Couette or Poiseuille flow and each Sc. A schematic illustration of the computational box and particle trajectories is shown in Fig. 1.

C. Post processing of data

The data for particle position, velocity, vorticity, and the derivative of the fluid velocity at the particle location in three directions were obtained and recorded for every particle in the flow and at every time step. To calculate the fluctuating velocity and the derivative of the fluctuating velocity at each time step, the profile of the mean velocity $\overline{U}$ and the derivative of this velocity $d\overline{U}/dy$ in the Eulerian frame were used. Linear interpolation was then applied to obtain the mean velocity values at the corresponding Y position for each particle. The relative normalized helicity density $h' = \cos\theta'$, where θ' is the angle between the fluctuating velocity and vorticity vectors,[35] was calculated as follows:

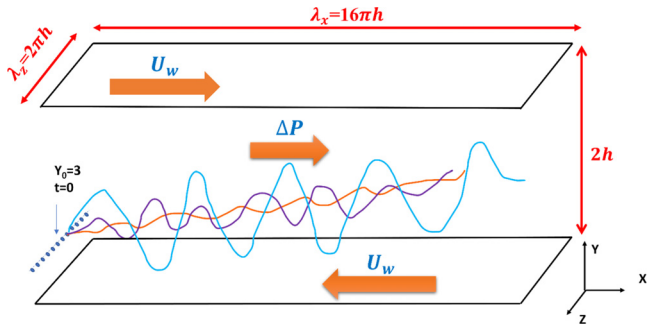

FIG. 1. This is a sketch of the set-up of the simulation with the computational box and the trajectories of particles. The blue line is a particle with large Brownian motion at small Schmidt number ($Sc = 0.7$), the purple is at $Sc = 6$ and the red line is the case of fluid particles. The illustration is shown for Poiseuille flow ($U_w = 0$, $dP/dx \neq 0$) and Couette flow ($dP/dx = 0$, $U_w \neq 0$).

$$\cos\theta' = \frac{\boldsymbol{u}' \cdot \boldsymbol{\omega}'}{(|\boldsymbol{u}'||\boldsymbol{\omega}'|)}, \tag{3}$$

where $\boldsymbol{u}' = \boldsymbol{u} - \overline{\boldsymbol{U}}$ and $\boldsymbol{\omega}' = \nabla \times \boldsymbol{u}'$ are the fluctuating velocity and vorticity, respectively.

The statistical analysis was based on calculations of correlation coefficients and joint probability density functions (JPDF) to demonstrate how h' was distributed for all values of the fluctuating velocity in the y direction, v'. In this case, to calculate the JPDF $P(v', h')$, a 2D array of bins was generated that spanned the range of values of v' and h'. We also calculated the JPDF defined as $P(\cos(\alpha), h')$, where α was the angle between the vorticity vector and the vertical direction y, in order to probe the correlation of this angle and h'. The number of scalar markers that had values within the range of each bin was counted and then the probability was calculated by dividing with the total number of particles.

III. RESULTS AND DISCUSSION

A. Helicity and vertical velocity

In a previous study, we have analyzed subsets of scalar markers that had positive vertical velocity (i.e., these were particles moving away from the wall), against the markers that had negative vertical velocity and moved toward the wall. In general, these markers could contribute to the generation of turbulent scalar flux—the markers moving toward the wall could transfer mass from the channel center to the wall, while the markers that move away from the wall transfer mass from the bottom region of the channel to the outer region of the flow.[55]

Therefore, to investigate the role of helicity in scalar transport in turbulent flow, the correlation between helicity and vertical velocity needs to be considered. The JPDF between the relative helicity density, h', and vertical fluctuating velocity of all particles that were released at $Y_0 = 3$, 10, and 75 for Poiseuille and Couette flow at $Sc = 0.7$, 6 and fluid particles are shown in Figs. 2 and 3, respectively. These positions were selected because they correspond to release within the viscous wall sublayer (which extends to $Y = 5$), the buffer region between the viscous wall sublayer and the logarithmic region (which extends between $Y = 5$ and 35), and the logarithmic region of the flow. The data for the rest of the release locations can be seen in the supplementary material. The data for particles released at the center of the channel, at $Y_0 = 300$, look the same as the data for particles released in the

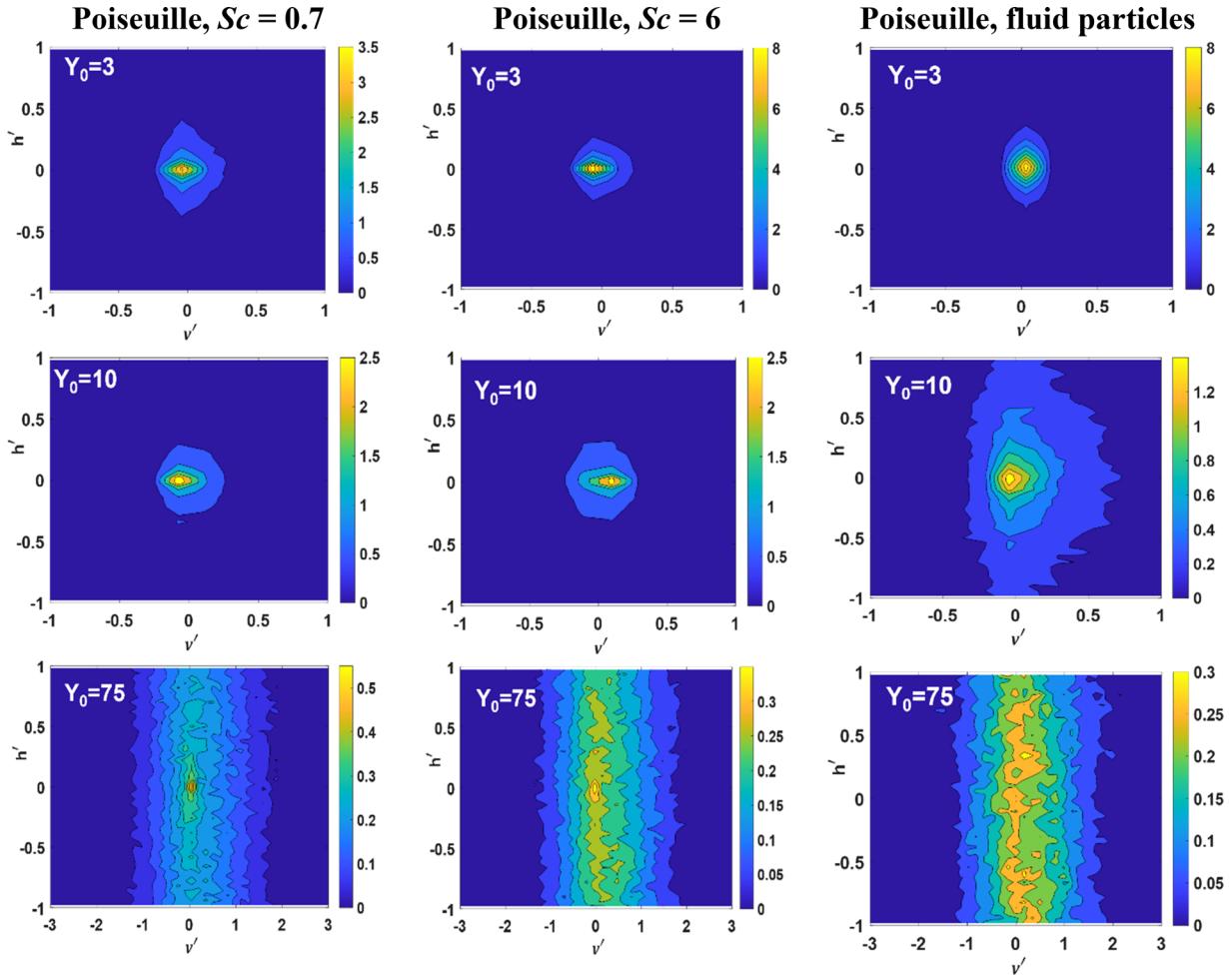

FIG. 2. JPDF of relative helicity density $h' = \cos\theta'$ and vertical velocity v' of all particles, at time $t = 100$ for Poiseuille flow at $Sc = 0.7$, 6, and fluid particles. Rows correspond to different locations of marker release in the y direction, indicated by the value of Y_0, shown in the plots, and columns correspond to markers of different Sc, as indicated at the top of the figure.

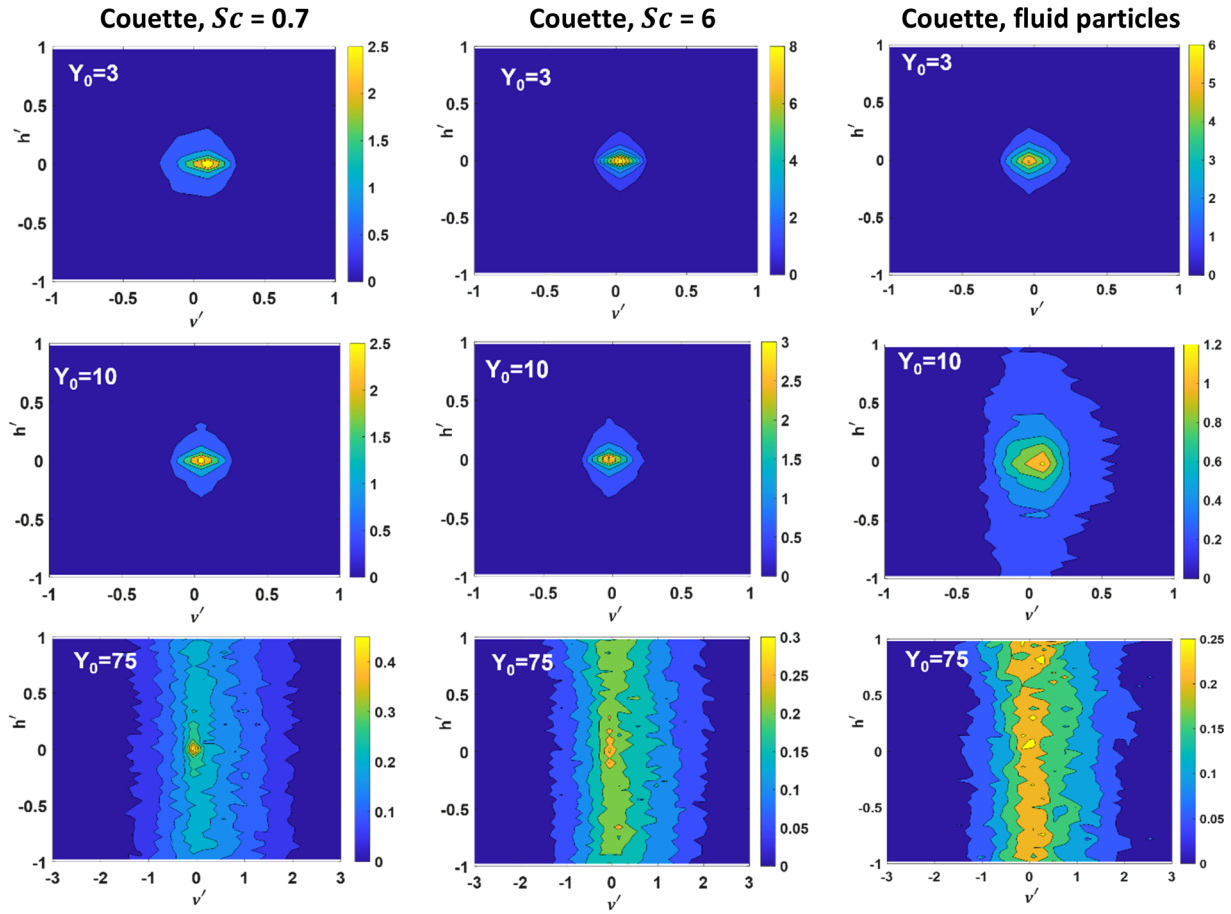

FIG. 3. JPDF of relative helicity density $h' = \cos\theta'$ and vertical velocity v' of all particles, at time $t = 100$ for Couette flow at $Sc = 0.7$, 6, and fluid particles. Rows correspond to different location of marker release in the y direction, indicated by the value of Y_0, shown in the plots, and columns correspond to markers of different Sc, as indicated at the top of the figure.

logarithmic layer at $Y_0 = 75$. As release positions get closer to the wall and inside the viscous wall sublayer, i.e., for $Y_0 = 3$, the values of both h' and v' are concentrated around zero. This means that in the near wall region, the fluctuating velocity vector and the fluctuating vorticity vector are mostly perpendicular to each other. Furthermore, the value of the vertical velocity is not significant to drive the particles away from the wall. However, when the release position is $Y_0 = 10$, the distribution of h' and v' extended to larger values than those for particles released close to the wall. The values of h' extended between -1 and 1 when the particles were released in the logarithmic layer at $Y_0 = 75$, indicating that the vorticity and velocity vectors become aligned to each other (i.e., the cosine of the angle between $\boldsymbol{u}'$ and $\boldsymbol{\omega}'$ is -1 or 1). In general, the distribution is relatively symmetric around $h' = 0$. From this evidence, it could be concluded that there is a correlation between the vertical velocity and helicity and this correlation is affected by the Sc and the location of particle release in the flow.

To provide more evidence about the correlation between helicity and vertical velocity, the particles that moved the farthest from the wall were separated from the particles that moved the less from the wall when released at $Y_0 = 3$. In this way, we want to focus on the flow characteristics that contribute the most to scalar transfer away from the wall. The JPDF was recalculated by selecting the top quartile—only 25% of the particles, those that were the farthest from the wall at $t = 100$ (see the bottom row in Figs. 4 and 5). In the top row of Figs. 4 and 5, the JPDF between h' and v' for the 25% of the particles that were the closest to the wall are shown. For particles closest to the wall, both h' and v' have values close to zero, between -0.1 and 0.1 for velocity and between -0.2 and 0.2 for helicity density. After being released, particles that do not disperse far remain in the near wall region, and in this region the velocity vector and vorticity vector are nearly perpendicular to each other. For the particles that disperse the farthest from the wall, the distribution of velocity and helicity is symmetric around $h' = 0$, and it appears to widen, showing that there is no tendency in the alignment between velocity and vorticity. This finding agrees with prior results about flow structures that contribute the most to turbulent transport.[56] Rotating eddies were found to contribute to transport close to the wall, but farther from the wall, the transport was through larger vertical structures, called plumes.[55] These were created as short eddies close to the wall would act as pumps to move the scalar away from the wall, where other eddies would take over the

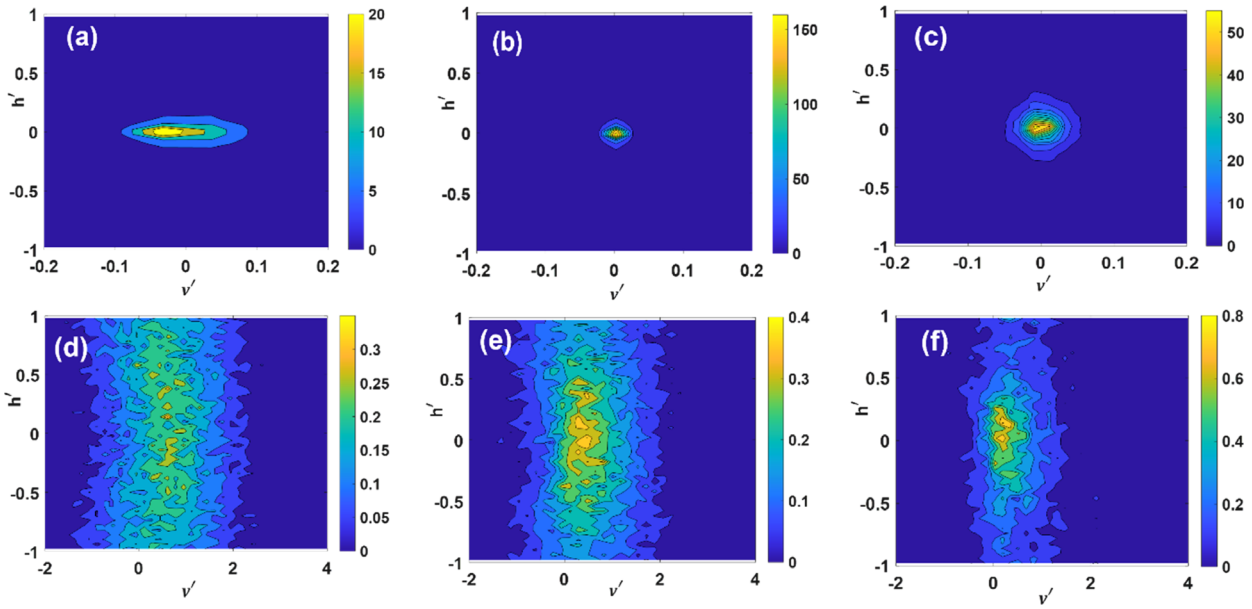

FIG. 4. JPDF of relative helicity density $h' = \cos\theta'$ and vertical velocity v' at $t = 100$ for only the quartile of particles in Poiseuille flow that are the closest to the channel wall (a) $Sc = 0.7$, (b) $Sc = 6$, and (c) fluid particles, and for the particle quartile that are the farthest from the wall (d) $Sc = 0.7$, (e) $Sc = 6$, and (f) fluid particles in Poiseuille flow from initial position $Y_0 = 3$.

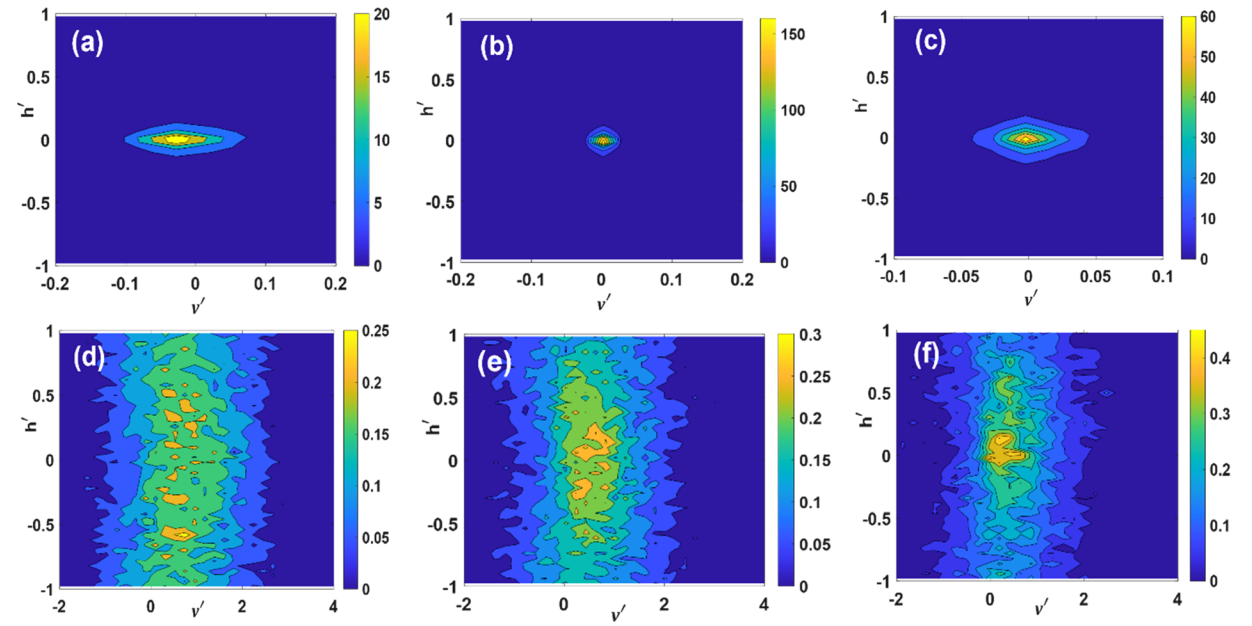

FIG. 5. JPDF of relative helicity density $h' = \cos\theta'$ and vertical velocity v' at $t = 100$ for only the quartile of particles in Couette flow that are the closest to the channel wall (a) $Sc = 0.7$, (b) $Sc = 6$, and (c) fluid particles and for the quartile of particles that are the farthest from the wall (d) $Sc = 0.7$, (e) $Sc = 6$, and (f) fluid particles in Poiseuille flow from initial position $Y_0 = 3$.

contribution to scalar transport. Since a collection of eddies rather than one type is responsible for transport, the angle between velocity and vorticity vector along the trajectories of the transported particles is more uniform. A large positive v', as seen in the bottom row of Fig. 4, could drive particles to move farther from the wall, and a negative velocity could bring particles back toward the wall. The range of values for h' tends to extend, and the distribution of h' tends to be more uniform between -1 and 1.

B. Helicity and orientation of vorticity

In this section, we investigate the relation between the direction of the vorticity vector for the fluctuating velocity and the relative helicity density. The direction of $\boldsymbol{\omega}'$ is calculated by considering the angle α between $\boldsymbol{\omega}'$ and the y direction that is normal to the channel walls. In this way, when $\boldsymbol{\omega}'$ is oriented in the streamwise or spanwise directions, the cosine of α is zero and when $\boldsymbol{\omega}'$ is normal to the wall, the cosine of α is either one or minus one. Flow structures that have α between 0° and 90° are most likely associated with ejection or sweep events in the buffer and logarithmic regions of the flow. This correlation between helicity and the angle of the vorticity vector relative to the vertical direction can be visualized by calculating the JPDF for these two quantities. The $\cos\alpha$ can be calculated as follows (w_i is the vorticity component in x, y, and z directions as indicated by the index i):

$$\cos\alpha = \frac{w_y}{\sqrt{|w_x|^2 + |w_y|^2 + |w_z|^2}}. \tag{4}$$

Figures 6 and 7 present the JPDF of relative helicity density $h' = \cos\theta'$ and $\cos\alpha$ for all particles of Poiseuille and Couette flows for $Sc = 0.7$, 6 and the fluid particles. Particles released within the near wall region show a distribution of $\cos\theta'$ and $\cos\alpha$ just within a small range of values between −0.2 and 0.2. See the supplementary material for more data on all release positions. The small values of $\cos\alpha$ and $\cos\theta'$ indicate that the vorticity is perpendicular to the vertical axis of the channel and is also perpendicular to the velocity vector, indicating that the fluctuating velocity vector of markers released in the near wall region tends to align with the direction that is normal to the wall [see the sketch in Fig. 8(d)]. This means that the flow vortices tend to move along the streamwise or spanwise direction while in the near wall region, but the particles would disperse along the vertical direction. The shape of the JPDF is symmetric and looks like a circle. When scalar markers were released farther from the wall, the distribution extended to larger values for both $\cos\theta'$ and $\cos\alpha$ and the JPDF for fluid particles indicates the most extension. Figure 8 is an illustration for the alignment between vorticity and velocity

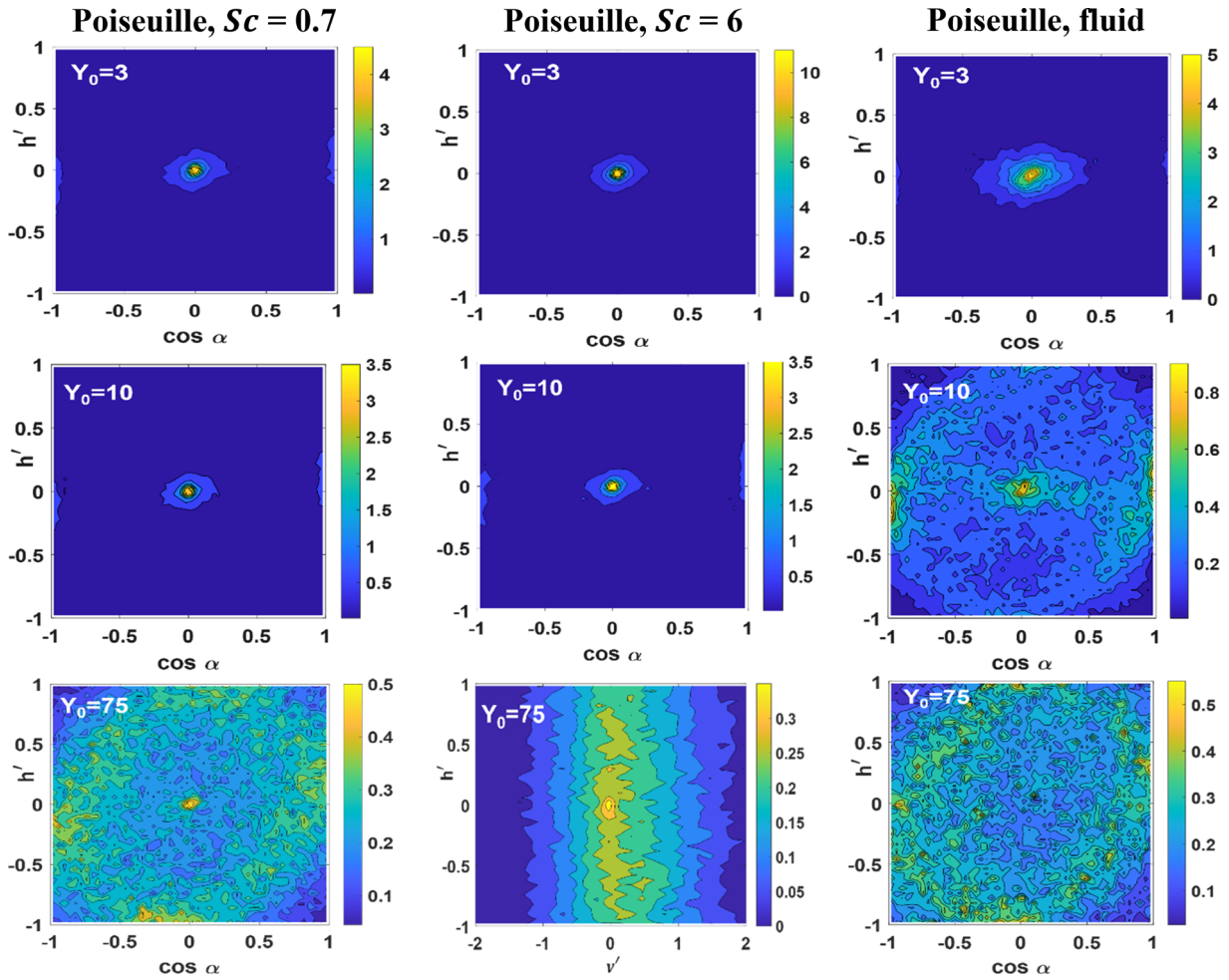

FIG. 6. The JPDF of relative helicity density $h' = \cos\theta'$ and the cosine of the angle between vorticity and the normal direction $\cos\alpha$ of all particles and Poiseuille flow at $t = 100$. Rows correspond to different locations of marker release in the y direction, indicated by the value of Y_0, shown in the plots, and columns correspond to markers of different Sc, as indicated at the top of the figure.

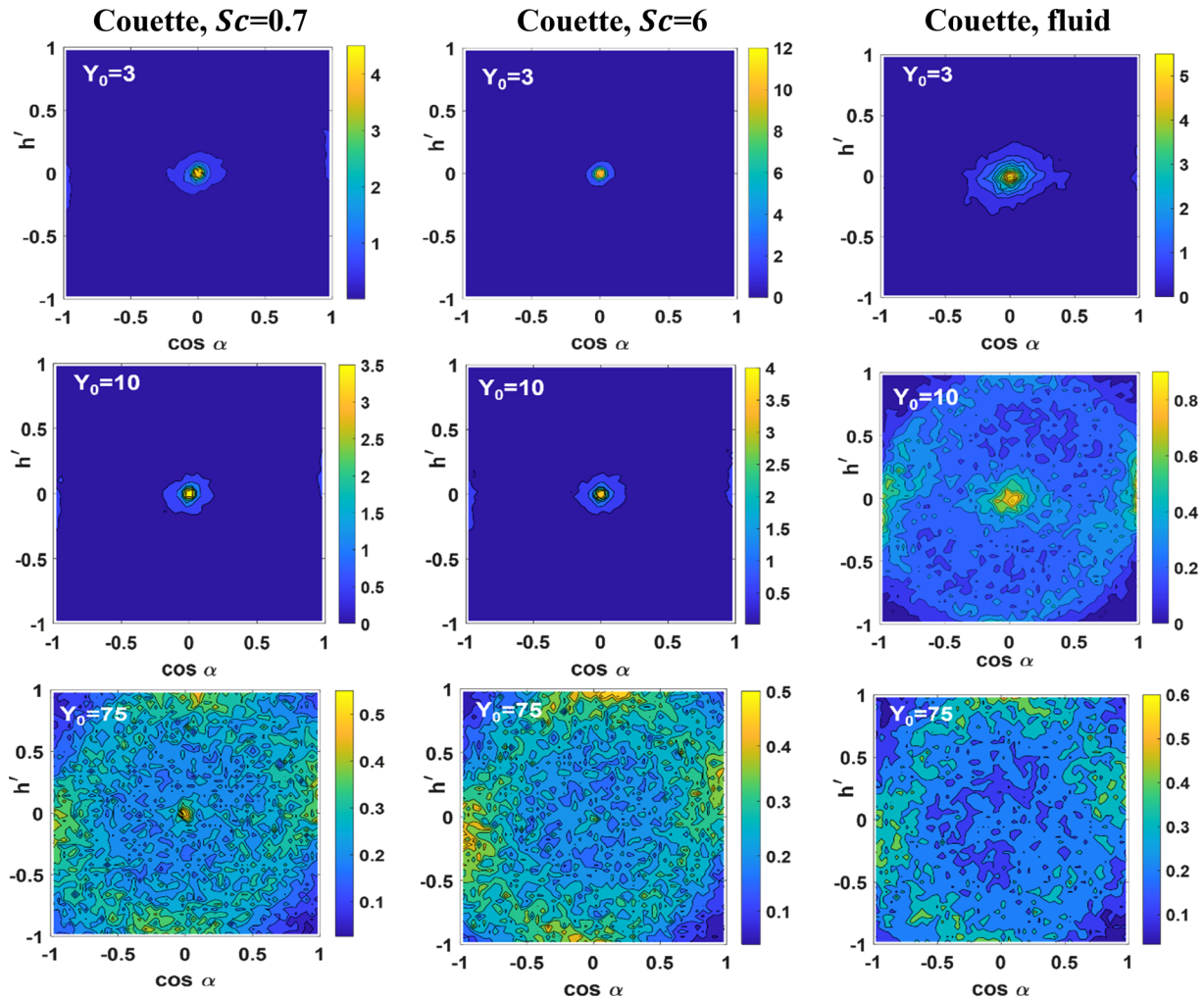

FIG. 7. The JPDF of relative helicity density $h' = \cos\theta'$ and the cosine of the angle between vorticity and the normal direction $\cos\alpha$ of all particles and Couette flow at $t = 100$. Rows correspond to different locations of marker release in the *y* direction, indicated by the value of Y_0, shown in the plots, and columns correspond to markers of different *Sc*, as indicated at the top of the figure.

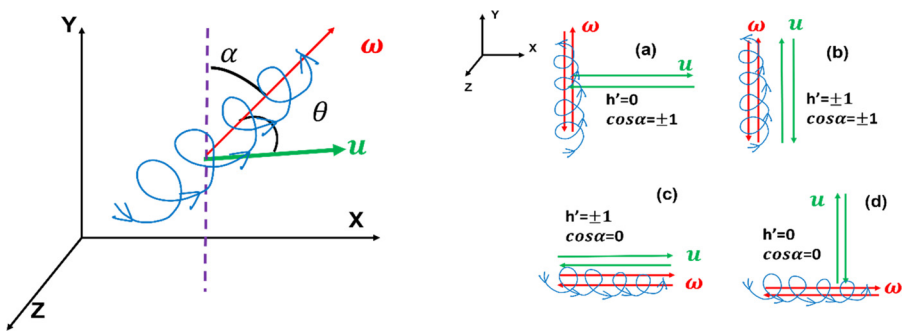

FIG. 8. This is an illustration of the alignment of the fluctuating vorticity and velocity vectors that define the values of $h' = \cos\theta'$ and $\cos\alpha$. (a) A case where vorticity and velocity vectors are perpendicular to each other, and vorticity is in the *y* direction. The velocity convects the eddy in the *x* direction. (b) Case where the velocity and vorticity vectors are aligned to each other and the vertical direction, and the velocity convects the vorticity in the *y* direction. (c) A case where the velocity and vorticity vectors are aligned to each other and the in the *xz* plane; and (d) a case where vorticity and velocity vectors are perpendicular to each other, and velocity is in the vertical direction while vorticity is in the streamwise or spanwise direction.

vectors, and a visual representation of the angles θ' and α that determine $h' = \cos\theta'$ and $\cos\alpha$.

For release within the logarithmic layer region and in the channel center (shown in the supplementary material), the distribution looks more uniform, and there is no certain shape for the contours of the JPDF. This is evidence that the distribution of h' changes with the position of particle release and with the *Sc*, but the flow configuration (Poiseuille or Couette) does not have a significant effect on this.

C. Relative helicity density and Reynolds stress quadrants

In this section, the distribution of relative helicity density conditioned on each of the four Reynolds stress quadrants for Poiseuille and Couette flow at different *Sc* numbers at time $t = 100$ is investigated to probe further the relation between helicity and coherent structures in anisotropic turbulent flow. Quadrant analysis of the Reynolds shear stress is typically employed for the identification of coherent structures, and to separate ejection from sweep events.[57–60] The ejection and sweep events are coherent vortical structures that are generated in the near wall region and extend toward the logarithmic layer.[61] They move low momentum fluid to regions of high momentum and vice versa generating turbulent kinetic energy. These structures extend to the edge of the logarithmic region and become scarce at the center of the channel for Poiseuille flow.[62] For Couette flow, they can extend farther out, since the Couette flow channel exhibits a logarithmic layer that extends from one wall to the other, across the channel center.[63,64] Turbulent events associated with each quadrant are called outward interactions (quadrant 1, Q1, $u' > 0$ and $v' > 0$), ejections (quadrant 2, Q2, $u' < 0$ and $v' > 0$), downward interactions (quadrant 3, Q3, $u' < 0$ and $v' < 0$), and sweeps (quadrant 4, Q4, $u' > 0$ and $v' < 0$).[65] The forward dispersion in time through the viscous sublayer (i.e., dispersion from a point toward other regions of the turbulent flow) has behavior associated with transport due to Q2 or Q4 flow events. For backward dispersion in time (i.e., when one examines where particles were before arriving at a specific location in the turbulent flow field), the markers seem to be carried toward the viscous sublayer by Q1 or Q3 events at large times and by Q2 and Q4 events at small times. For Poiseuille flow, Kähler showed that the probability of finding high momentum fluid moving toward the wall (Q4-sweep events) is quite high when compared to high-speed fluid moving away from the wall.[66]

It can be seen from Fig. 9 that there is no significant difference of distribution of h' across the four quadrants, except for the release position at $Y_0 = 75$. The distribution of h' shows a peak close to the value of zero, indicating that the two vectors (velocity and vorticity) are perpendicular to each other in the near wall region [this could be cases (a) or (d) shown in Fig. 8]. The distributions become flatter when the particles were released farther from the wall. In addition, as the *Sc* decreases, the peaks appear to widen. This means that the distribution of h' along the trajectories of scalar markers does not depend on the Reynolds stress quadrant, but it depends on the particle position of release in the channel and on the molecular diffusivity of the particles.

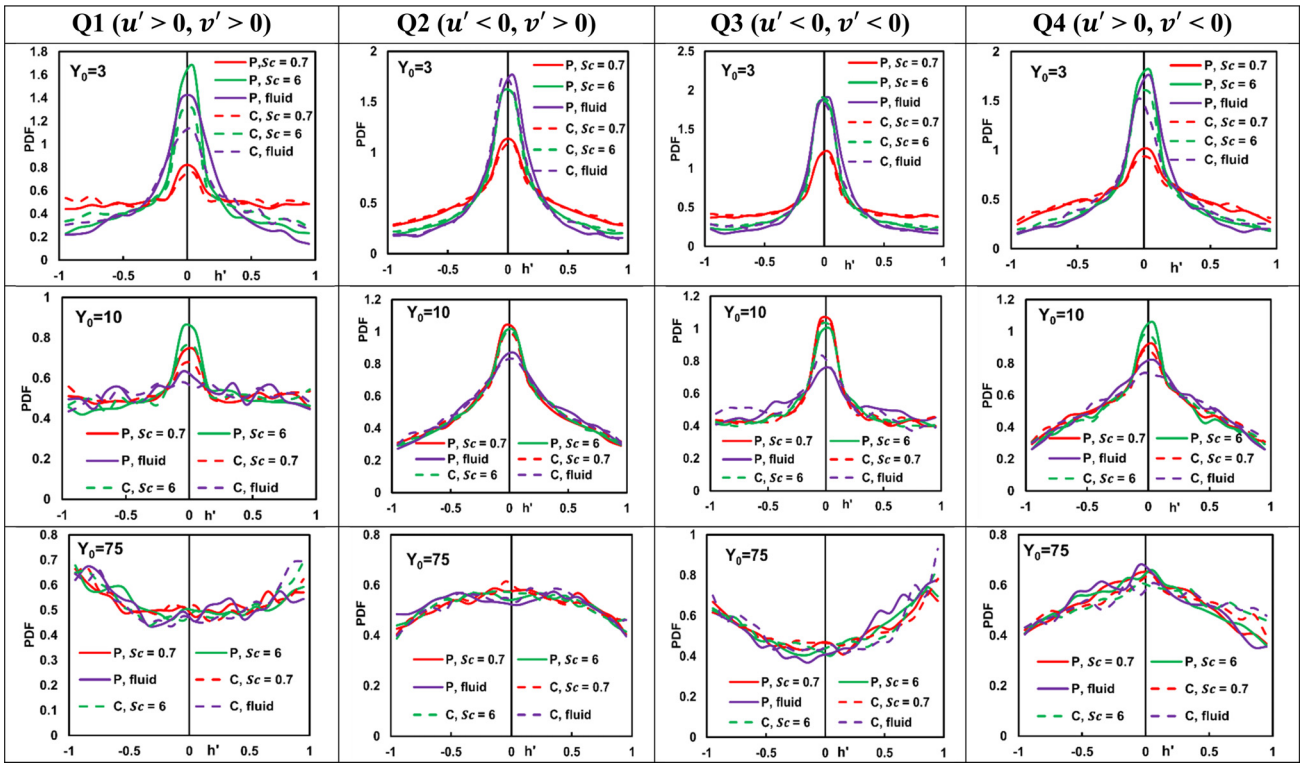

FIG. 9. Conditional distribution of relative helicity density $h' = \cos\theta'$ for particles within each of the four quadrants of Reynolds stress ($u'v'$) at $t = 100$. Rows correspond to different locations of marker release in the *y* direction, indicated by the value of Y_0, shown in the plots, and columns correspond to markers at different Reynolds stress quadrants at time $t = 100$. The type of flow, Poiseuille or Couette, is indicated by P or C, respectively, and the *Sc* is also indicated in the figure legends for each curve.

At release position of $Y_0 = 75$, there is a difference between quadrants Q2, Q4 and Q1, Q3. Although the distribution is quite flattened in this region, there are more particles in quadrants Q2 and Q4 that have values of h' close to zero, while the number of particles that have h' at -1 or 1 is more significant in cases of Q1 and Q3. Alignment of vorticity and velocity, indicated by values of h' close to 1 or -1, is taking place along the trajectories of particles in the logarithmic layer and beyond. In general, helicity density along the Lagrangian trajectories of scalar markers appears to be independent of the coherent structures as determined by Reynolds stress quadrant events.

The fluctuating velocity vector in a typical yz plane of the simulated flow is shown in Figs. 10 and 11. The particle positions are superimposed, colored with the value of h'. As can be seen, the particles appear to concentrate at the edges of vortical structures. This is more obvious in the case of $Sc = 6$, while the $Sc = 0.7$ particles disperse more uniformly. More importantly, near the wall region, the color of the particles shows that they reside in locations where the value of h' is around zero, and farther from the wall their color is blue or yellow, which indicates that the value of h' is distributed toward -1 or 1. Around vortices in the near wall region, most particles have green

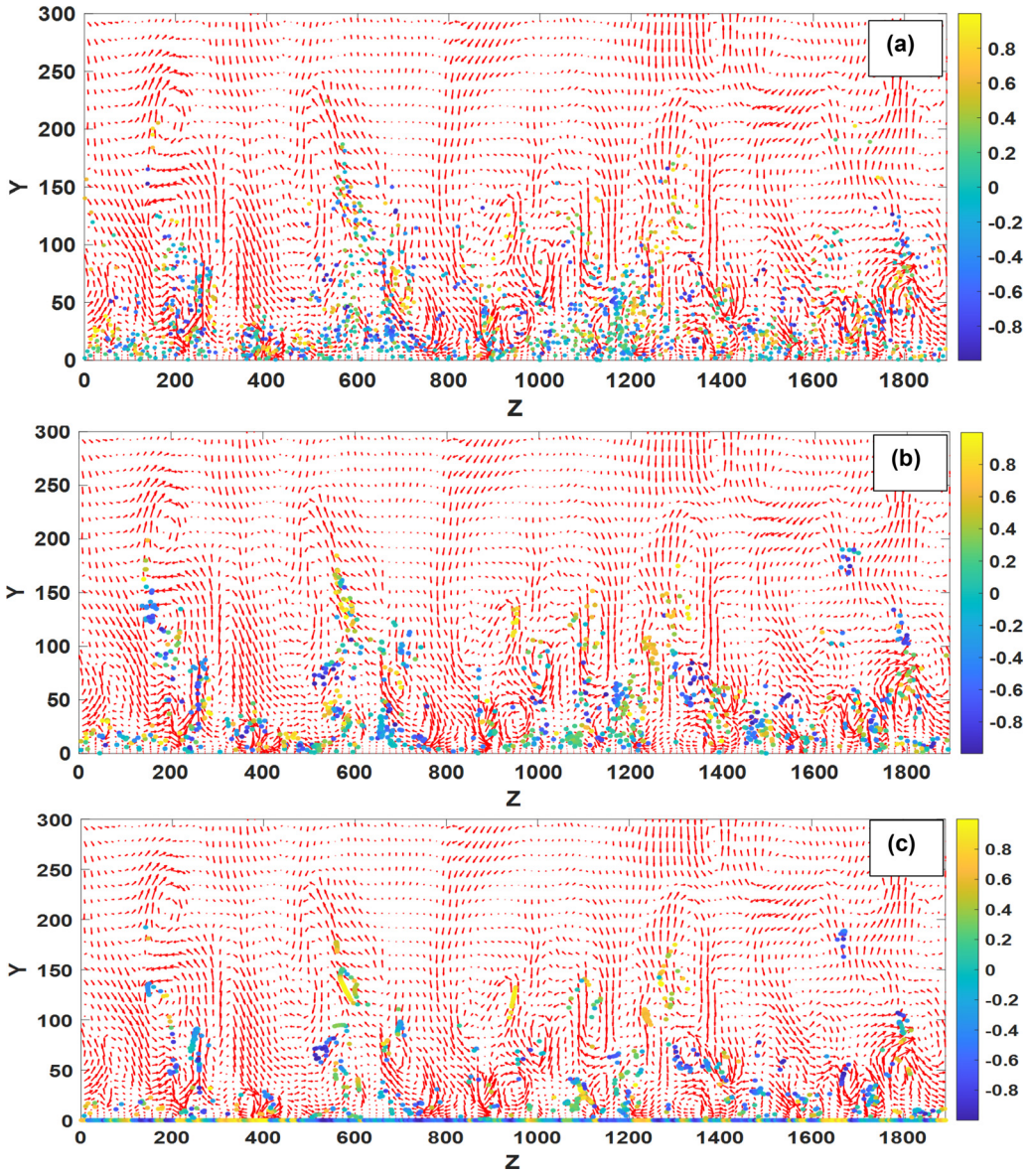

FIG. 10. Particle positions colored with h' superimposed on the vector plot of the velocity field at the normal-spanwise plane (yz plane) at $x = 3786$ and time $t = 100$ for Poiseuille flow at various Sc numbers (a) $Sc = 0.7$, (b) $Sc = 6$, and (c) fluid particles. The center of the channel is at $Y = 300$ and the bottom wall is at $Y = 0$. Particles found between 3769 $(254\,\Delta x) \leq x \leq 3799\,(256\,\Delta x)$ are shown.

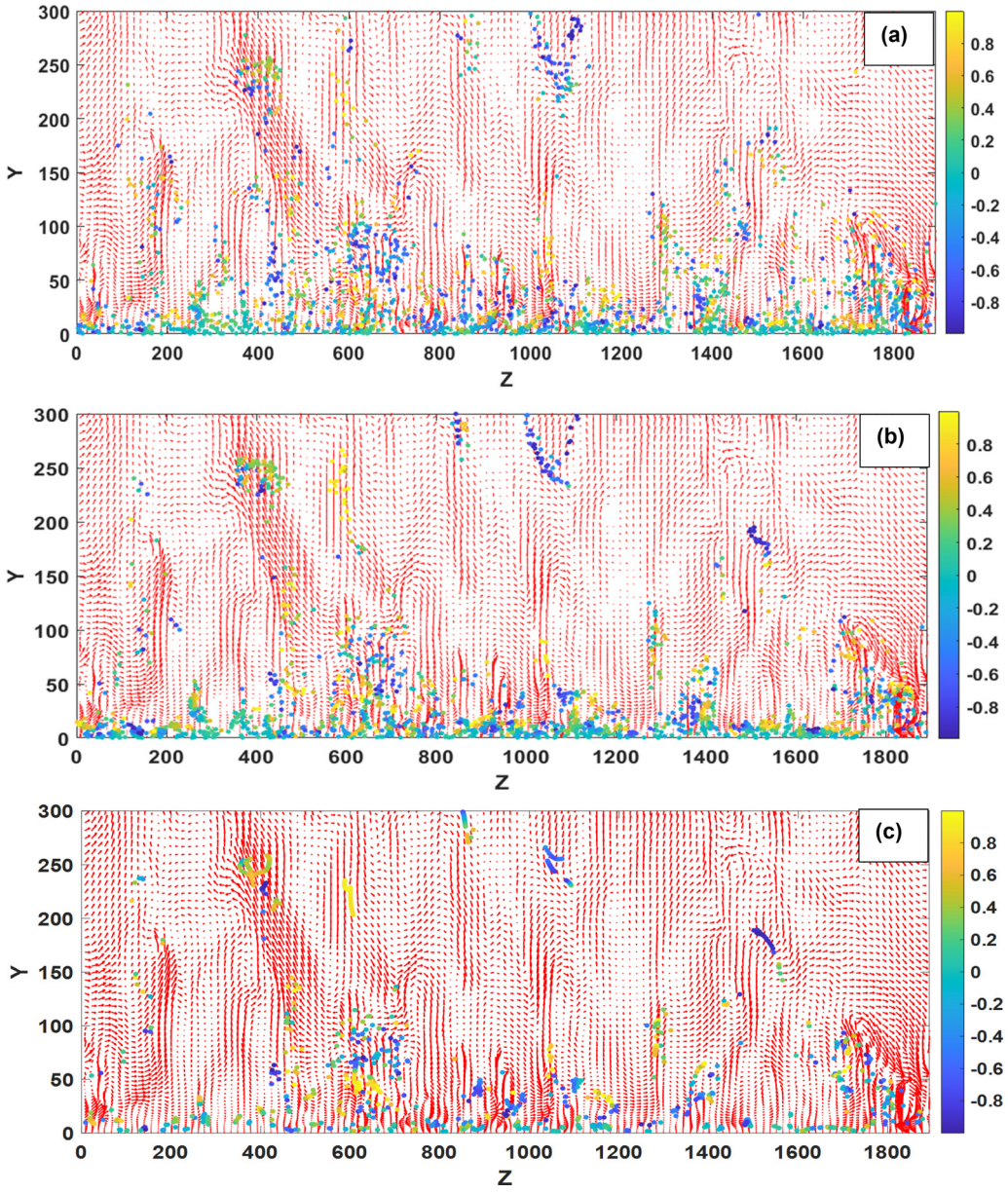

FIG. 11. Particle positions colored with h′ superimposed on the vector plot of the velocity field at the normal-spanwise plane (yz plane) at $x = 3786$ and time $t = 100$ for Couette flow at various Sc numbers (a) $Sc = 0.7$, (b) $Sc = 6$, and (c) fluid particles. The center of the channel is at $Y = 300$, and the bottom wall is at $Y = 0$. Particles found between $3769\,(254\,\Delta x) \leq x \leq 3799\,(256\,\Delta x)$ are shown.

color that indicates velocity and vorticity vectors that are perpendicular to each other.

D. Helicity and the Q-criterion for vortex identification

One of the criteria typically used to identify vortices is the Q-criterion that is based on the invariants of the rate of strain tensor and the vorticity tensor. The value of Q is determined as follows:[67,68]

$$S_{ij} = \frac{1}{2}\left(\frac{\partial u_i'}{\partial x_j} + \frac{\partial u_j'}{\partial x_i}\right), \tag{5}$$

$$\Omega_{ij} = \frac{1}{2}\left(\frac{\partial u_i'}{\partial x_j} - \frac{\partial u_j'}{\partial x_i}\right), \tag{6}$$

$$Q = \frac{1}{2}\left(\|\Omega\|^2 - \|S\|^2\right), \tag{7}$$

where u_i' is the fluctuating velocity in the i direction, S_{ij} is the ij component of the rate of strain tensor, and Ω_{ij} is the ij component of the vorticity tensor. The use of the Q value is suitable for the identification of vortices, since a value of $Q > 0$ indicates that rotation overcomes strain, ensuring the existence of a vortex structure that is protected from deformation.[31]

Relating helicity and vortices identified utilizing the Q-criterion has not been explored in the literature for turbulent flows. In a prior study, however, Povitsky *et al.* studied flow in a three-dimensional (3D) cubic cavity driven by moving the parallel walls in perpendicular directions to elevate helicity. They examined the helicity density, kinematic vorticity number, and normalized helicity density for flow with Reynolds number in the range of 100–1000. They also used the Q-criterion to identify vortices, but they did not correlate helicity with values of the Q-Criterion.[10]

Herein, the data generated by the DNS and the LST allow for a deeper investigation of the relationship between vorticity and helicity by utilizing the Q-criterion. The Lagrangian autocorrelation coefficient for Q is calculated for particles released at different distances from the channel wall. This coefficient, along the trajectories of particles, can be used to determine the time scales associated with particle transport in vortical structures and compare it to the time scales in the rest of the fluid. The Lagrangian autocorrelation is calculated as follows:[69]

$$R_{Q-Q(t)} = \frac{\overline{Q(t_0)Q(t_0+t)}}{\overline{Q(t_0)^2}^{1/2}\overline{Q(t_0+t)^2}^{1/2}}. \quad (8)$$

Figure 12 is a presentation of the autocorrelation for the Q values in Poiseuille and Couette flow at various Sc and particle release positions. The correlation coefficients remain larger than zero in the case of fluid particles and the values are around 0.1 at $t = 100$. The values of the correlation coefficient for Poiseuille flow are greater than those for Couette flow. Farther from the wall, the correlation decreases at a lower rate, as seen for particles released at $Y_0 = 75$. The correlation values decrease dramatically from initial time to $t = 100$ for the case of $Sc = 0.7$ and to $t = 20$ for $Sc = 6$ and fluid particles. The larger molecular dispersion for low Sc is the reason for this observation—the particles jump away from convective flow structures and disperse faster, decorrelating from the flow structure at which they were released at time zero. Note that the value of the correlation coefficient approaches zero for $Sc = 0.7$ at time $t = 100$. The fluid particles exhibit the longest correlation with time. Therefore, the Q values are correlated longer for Poiseuille flow and for larger Sc numbers.

While the results appearing on Fig. 12 provide general information for all particles, showing that low Sc results in enhanced transfer, Fig. 13 is focused on discriminating between the particles that disperse the most compared to the particles that disperse the least in the y direction. To probe differences in the flow structures that move particles away from the wall, the correlation of Q values for the particles that are found the farthest away and those that are found the closest to their release location at $Y_0 = 3$ are shown in Fig. 13. In general, the correlation coefficient values are larger than zero, and the correlation profile looks smoother for the particles that do not disperse far in the y direction. As expected, the particles of Poiseuille and Couette flows at $Sc = 0.7$ have the fastest decrease in the correlation coefficient value, followed by the $Sc = 6$ and the fluid particles. The fluid particles present periodicity in the values of the correlation both in Couette and

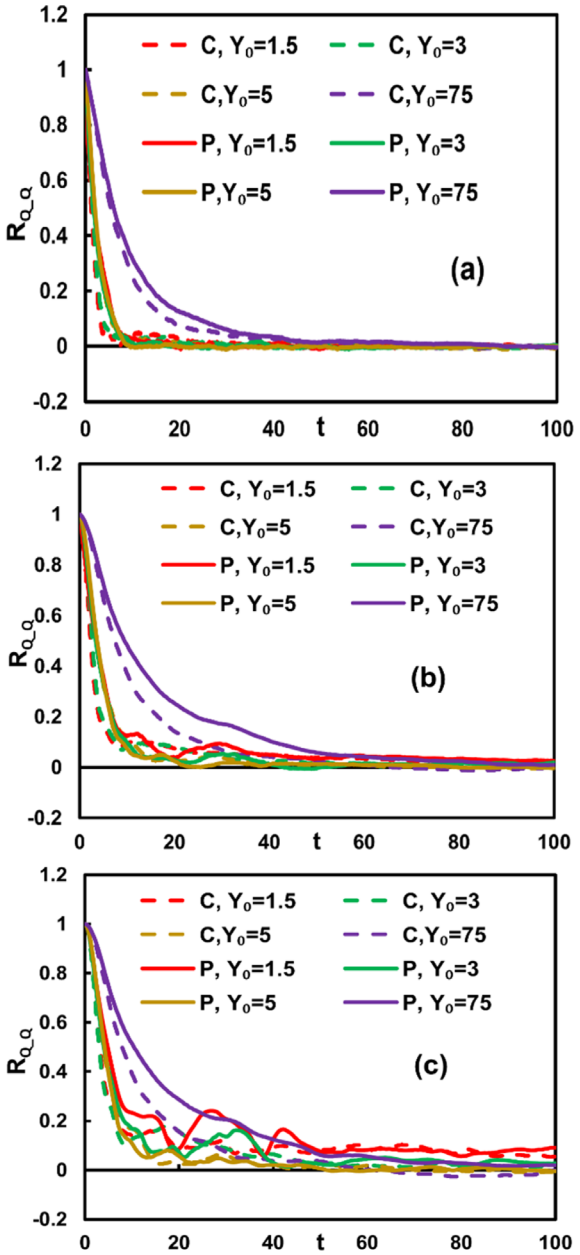

FIG. 12. The autocorrelation coefficient for the Q values as a function of time for Poiseuille and Couette flow (indicated as P and C on the legend) at various Sc numbers and for different positions of particle release (a) $Sc = 0.7$, (b) $Sc = 6$, and (c) fluid particles.

Poiseuille flows. More importantly, it can be concluded that the particles that have the least dispersion for the same Sc are those that have the longer correlation of the Q-criterion values. This is because they remain within flow structures that are still in the near wall region, where coherent structures dominate, while the particles that disperse the most leave these coherent structures and move farther from the wall. This result corroborates the findings of Karna and Papavassiliou

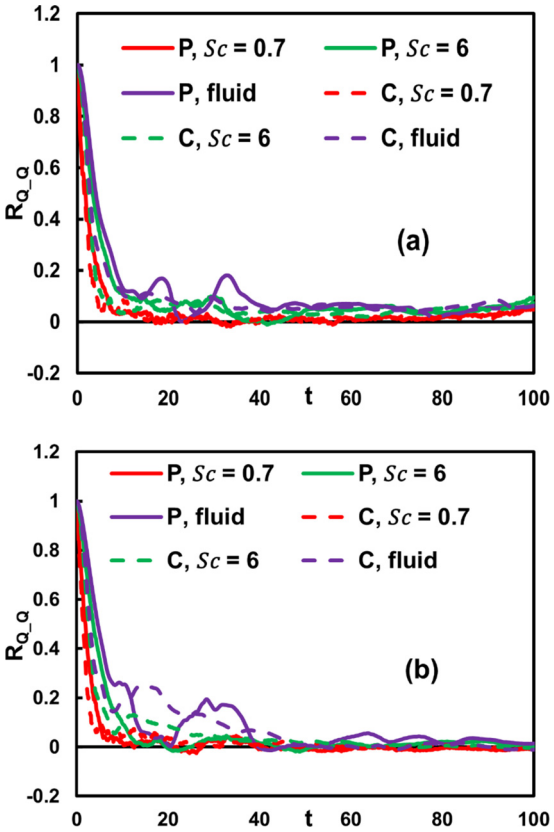

FIG. 13. The correlation of Q values with time for particles conditional on their location relative to the wall at time $t = 100$: (a) The quartile of all particles that are closer to the wall, (b) the quartile of particles that are the farthest from their initial position at $Y_0 = 3$ for Poiseuille and Couette flow and for various Sc.

that scalar transport away from the wall is the result of the combined effect of more than a single eddy.[56] Since the autocorrelation for the Q-criterion goes to zero, it means that the markers stop being associated with the vortex in which they were released, and their dispersion occurs by other flow structures.

The distribution of relative helicity density conditioned on $Q > 0$ is analyzed at different release positions and Sc numbers and shown in Fig. 14. In general, the distribution of h' varies with the change of Sc numbers and position of particle release. The fluid particles have the highest probability of zero value of h' at the release position $Y_0 = 1.5$ and then the peak decreases gradually as Y_0 increased. The particles with $Sc = 6$ exhibit similar trends, as do fluid particles. The case of $Sc = 0.7$ also indicates a change with the position of release but the distribution is flatter in comparison to the distributions for $Sc = 6$ and for fluid particles. On the other hand, the distribution of h' is almost a uniform distribution at $Y_0 = 75$, which means that there is no representative characteristic helicity in this region despite the fact that the particles are within vortex regions ($Q > 0$). Once again, there appears to be no clear correlation between the values of helicity density and the vortex structure. The alignment of vorticity and velocity vector, expressed by the helicity density, depends mainly on the regions within which particles disperse. At release positions close to the wall, vorticity and velocity are perpendicular to each other, and as the particles disperse away from the wall, the vorticity and velocity tend to become parallel to each other.

E. Relative helicity density and strain rate tensor

According to Zhang *et al.*, helicity density has been considered as a vortex identifier, however, helicity density is not Galilean invariant.[70] This is a valid criticism for this approach, since this criterion is not applicable for general nonhomogeneous turbulent flows. The principal directions (i.e., the eigendirections) embedded in the flow structures are, thus, important. For a vortex, the eigendirections of the rate of

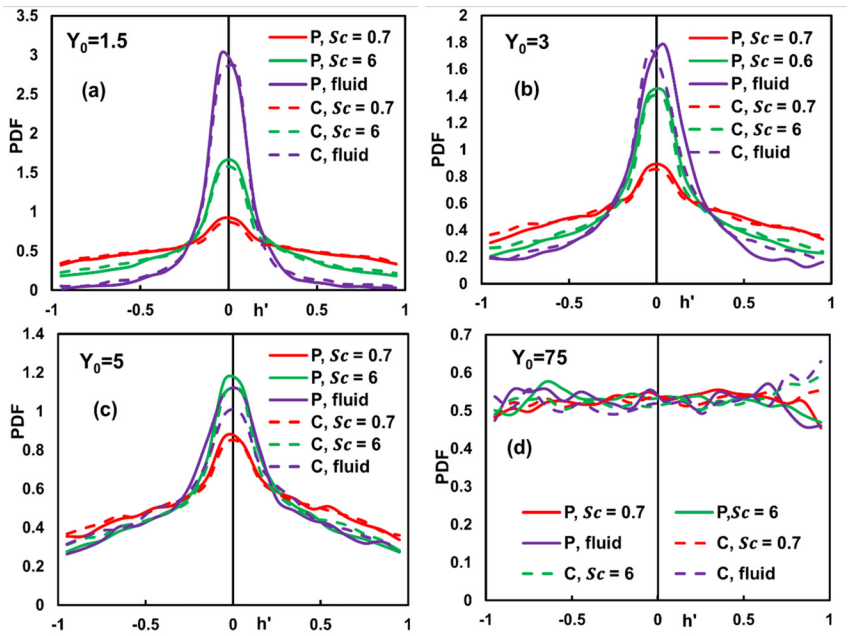

FIG. 14. The distribution of relative helicity density h' conditioned for $Q > 0$ for Poiseuille and Couette flows at various Sc numbers and for release positions (a) $Y_0 = 1.5$, (b) $Y_0 = 3$, (c) $Y_0 = 5$, and (d) $Y_0 = 75$ at time $t = 100$.

strain tensor can be used, because this tensor produces real eigenvalues and eigenvectors.[70,71] The eigenvalues of the rate of strain tensor can be ordered in size as $\lambda_1 \geq \lambda_2 \geq \lambda_3$ with the restriction that they sum to zero for incompressible flow.[72] In 3D incompressible flows, the principal directions consist of one extensive and one compressive direction, and an intermediate direction, which can be either extensive or compressive. Vorticity is preferentially aligned with the intermediate direction and typically misaligned with both the compressive direction and the extensive direction.[73]

Arhurst *et al.* studied the probability of vorticity alignment in isotropic flow and showed that vorticity is most likely to point in the λ_2 direction, and least likely to point in the most compressive direction λ_3. The eigenvector corresponding to the intermediate eigenvalue tends to be parallel to the vorticity vector.[74] The author also investigated the correlation between the eigendirections of the rate of strain tensor and vorticity and helicity and showed that there is a slight dependence in the shape of relative helicity PDFs when conditioned on λ_2.[72] The largest eigenvalue of the rate of strain, λ_1, is always positive and λ_3 is always negative, therefore the sign of λ_2 could determine whether the local structure of turbulence is sheetlike or tubelike. If $\lambda_2 > 0$, there are two components of the rate of strain along which the fluid is stretching, and one component along which it is compressed suggesting that the local structure will be sheetlike. Meanwhile, if $\lambda_2 < 0$ there will be two compressive components and one stretching component of the rate of strain, which suggests tubelike structures. On the other hand, this study showed that the dissipative structures of turbulence are sheets and when sheetlike structure is strongest, the influence of helicity is even smaller. The sheetlike structure is related to the nonlinear terms of the Navier–Stokes equation responsible for vortex stretching and the cascade of energy to small scales.[71] As described by Arhust *et al.*, there is a correlation between a diffusing scalar and the strain field when studying 2D mixing flows.[72] The PDF of the alignment between $\boldsymbol{\omega}$ and eigenvectors $\boldsymbol{e_i}$, $\cos(\boldsymbol{\omega}, \boldsymbol{e_i})$, in Nakamura *et al.*,[74] indicated that the shapes of the PDF do not depend much on time.

In the present study, the largest eigenvalue λ_1 of the rate of strain tensor, $S_{ij} = \frac{1}{2}\left(\frac{\partial u_i'}{\partial x_j} + \frac{\partial u_j'}{\partial x_i}\right)$, corresponds to eigenvector $\boldsymbol{e}_1$ and is related

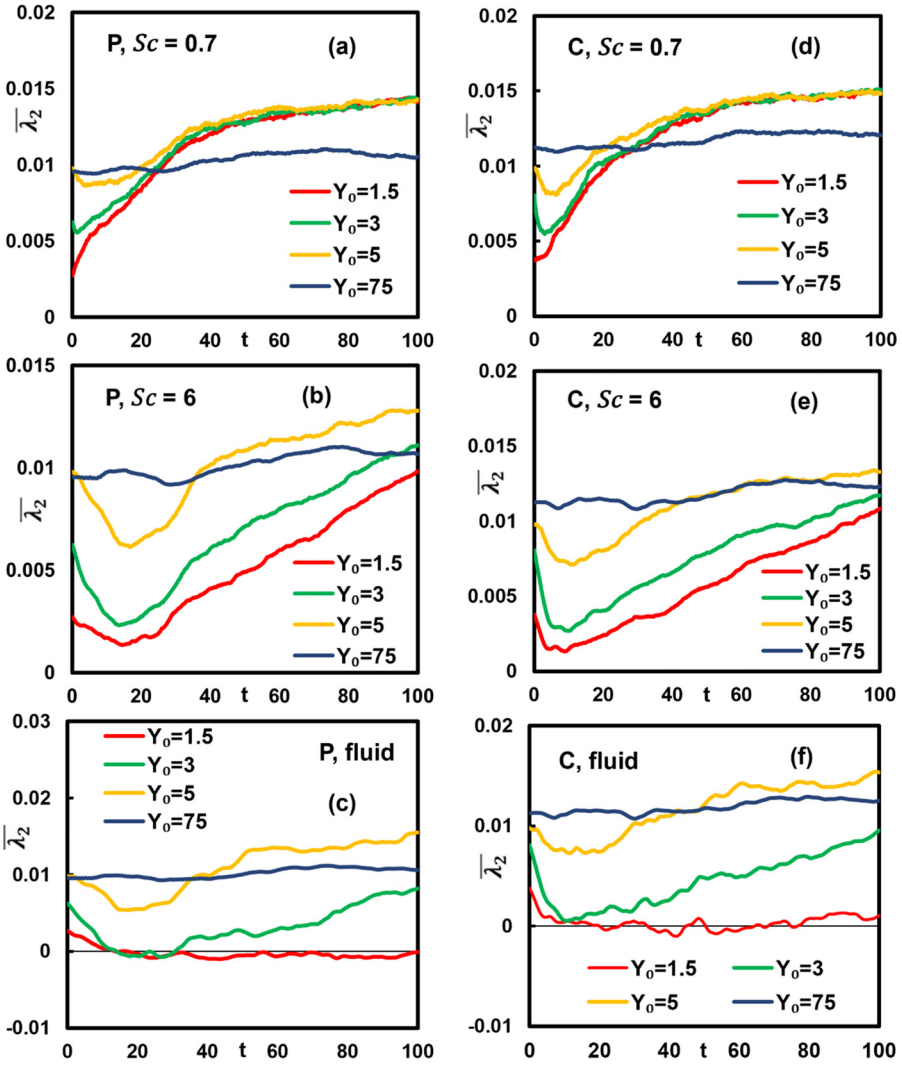

FIG. 15. The average value of the second largest eigenvalue λ_2 of strain rate tensor for Poiseuille (a) $Sc = 0.7$, (b) $Sc = 6$, and (c) fluid particles and in Couette flows (d) $Sc = 0.7$, (e) $Sc = 6$, and (f) fluid particles at various release positions.

to extension, λ_3 corresponds to eigenvector $\boldsymbol{e}_3$ and is related to compression, and λ_2 corresponds to eigenvector $\boldsymbol{e}_2$ and is related to either extension or compression.[73–75]

As discussed above, the value of λ_2 is directly related to the dissipative structures and, thus, it is important to evaluate the average value of λ_2 for passive markers moving in the flow field to understand further the effects of flow in enhancing turbulent transport. As can be seen from Fig. 14, the average value of λ_2 is larger than 0 as time advances, for both Couette and Poiseuille flows. The positive λ_2 corroborates earlier findings that the transport of scalars away from the wall is done more effectively in the form of sheet-like plumes[76] that transport the scalar markers away from the wall and that characteristics of these plumes depend on the Sc.[56] For the case of fluid particles, the average value of λ_2 does not show significant change with time, while at $Sc = 0.7$ and 6, it increases for particles released in the viscous sublayer, $Y_0 = 1.5$, 3, and 5. For particles released at $Y_0 = 75$, the average values of λ_2 do not seem to change for all cases, it is close to $\overline{\lambda_2} = 0.01$. The smallest values are observed when the release position was $Y_0 = 1.5$, and these values increased with the distance from the wall at $Y_0 = 3$ and 5. The positive values of λ_2 can be explained based on angular momentum conservation arguments. Indeed, for long times, the vorticity field is stretched out in the direction of the intermediate strain, which is positive and the other two vorticity components go to zero.[72]

While the average of λ_2 is positive, as indicated in Fig. 15, there are negative λ_2 values for some of the dispersing particles. Focusing on the distribution of relative helicity conditioned on $\lambda_2 > 0$, Fig. 16 was generated. The distribution curves depend on release positions and on Sc, which is a similar result as when considering unconditioned distributions and the distributions of h' conditioned on the Q-criterion. As mentioned already, positive values of λ_2 indicate sheet-like flow structures rather than tube-like flow structures that contribute to turbulent transport. As scalar markers travel along these structures, the peak of the distribution of h' is at zero for release in the viscous wall sublayer and high Sc, and velocity and vorticity are perpendicular to each other. For release outside the viscous sublayer or for high dispersion (for $Sc = 0.7$), the vorticity and velocity vectors have more uniform distribution of angles.

As discussed earlier, the λ_2 eigenvalue of the rate of strain tensor, or the Q-criterion, or the Reynolds stress quadrants have been used to indicate the existence of coherent structures. The distribution profiles reveal that there is not a distinction between conditioned or unconditioned distribution of relative helicity. Near to the channel wall, the peak of the PDF for h' is in values around zero, and father from the wall the values of h' start to become more uniform, leading to the flattening (widening) of the PDF peaks. On the other hand, the distribution of h' is affected by Sc, the smaller Sc numbers result in larger dispersion of particles that make the peaks of the distribution become flatter.

The cross correlation between relative helicity density h' and $\epsilon_i = |\cos(\omega, \boldsymbol{e}_i)|$ was calculated by the Pearson cross correlation formula as follows:

$$R_{h'-\epsilon} = \frac{\sum_{i=1}^{n}\left(h'_i - \overline{h'}\right)(\epsilon_i - \overline{\epsilon})}{\sqrt{\sum_{i=1}^{n}\left(h'_i - \overline{h'}\right)^2}\sqrt{\sum_{i=1}^{n}(\epsilon_i - \overline{\epsilon})^2}}. \tag{9}$$

Figures 17 and 18 are presentations of the cross correlation between the absolute value of $\cos\theta'$ and $\cos(\omega, \boldsymbol{e}_i)$ in the case of Poiseuille and Couette flows at $Sc = 0.7$, 6 and fluid particles. The absolute value of the cosine was used, since the important issue here is the alignment between the vectors, not which one is first or second when probing the angle between them. It can be seen that the cross correlation coefficients do not show significant change with time for $Sc = 6$ and the case of fluid particles, meanwhile the case of $Sc = 0.7$ has a remarkable change within the first 50 time units in the simulation. The correlation coefficient generally decreases when the particle release position was

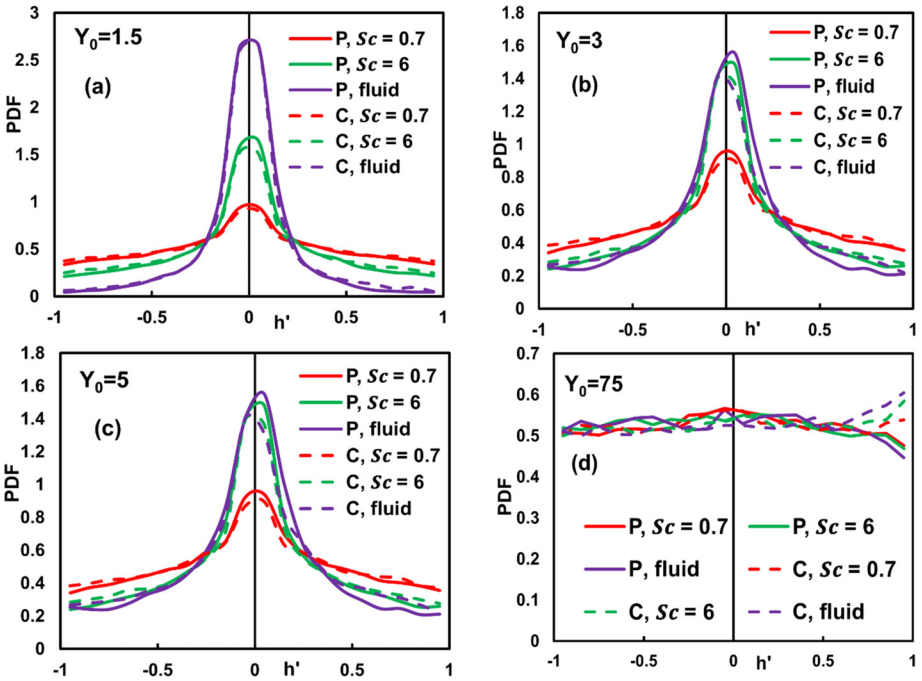

FIG. 16. Distribution of relative helicity density h' conditioned on $\lambda_2 > 0$ at various position of release (a) $Y_0 = 1.5$, (b) $Y_0 = 3$, (c) $Y_0 = 5$, and (d) $Y_0 = 75$ and Sc. Data at $t = 100$.

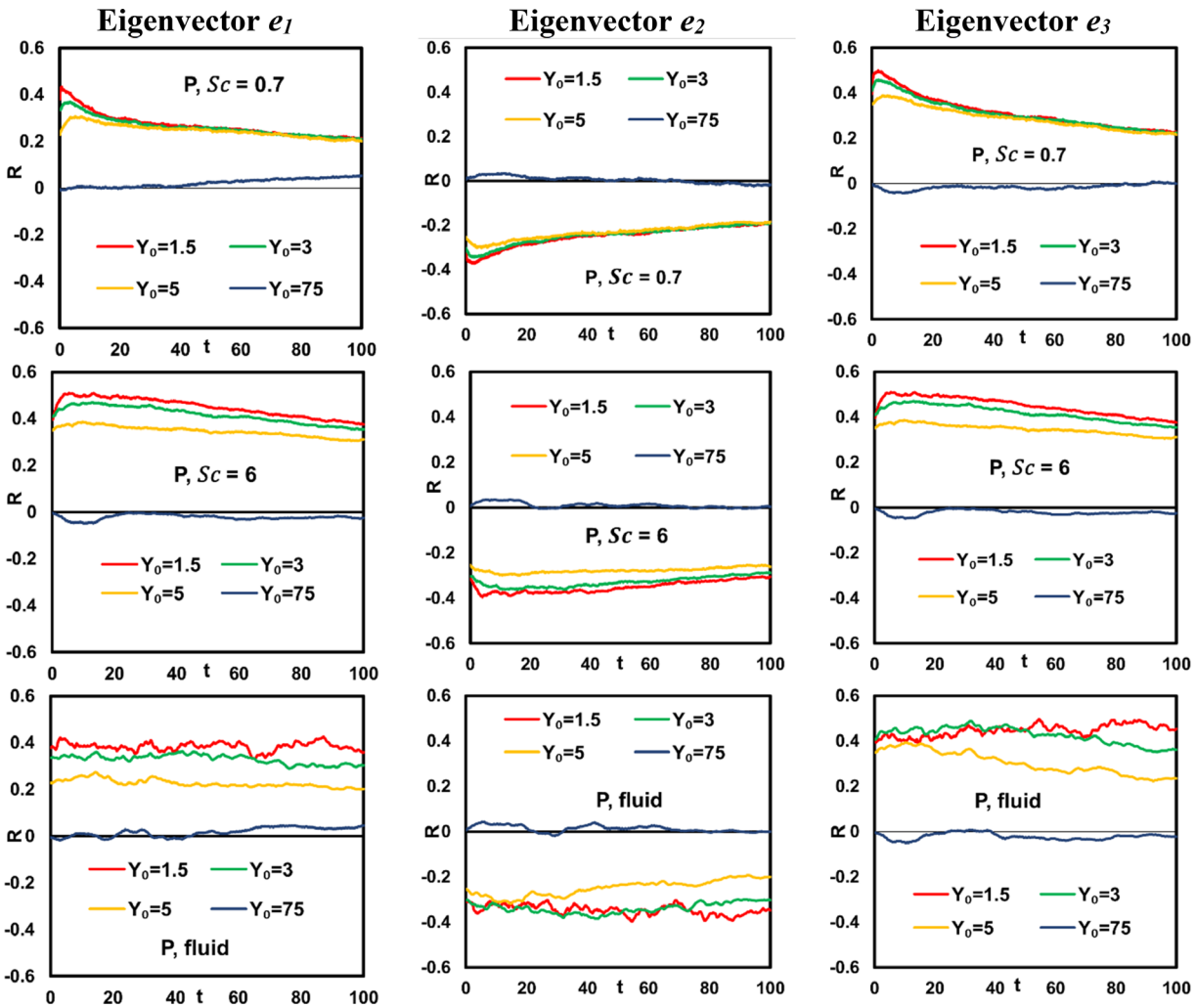

FIG. 17. Cross correlation between absolute value of relative helicity $h' = \cos\theta'$ and absolute value of the cosine between vorticity and the eigenvectors of the rate of strain tensor, $\cos(\omega, \mathbf{e}_i)$. $\mathbf{e}_i$ with i=1–3 corresponds to eigenvectors with eigenvalues $\lambda_1 \geq \lambda_2 \geq \lambda_3$, for Poiseuille flow and various Sc. Rows correspond to different Sc, while columns correspond to different eigenvectors.

located farther from the wall, and its value for release at $Y_0 = 75$ is approximately zero. This indicates that there is a correlation between the angle of vorticity projected on the eigenvectors of the rate of strain tensor, and that this correlation is different than zero for the duration of the simulations. More importantly, it is interesting that the values of the correlation between the absolute value of h' and $\cos(\omega, \boldsymbol{e}_2)$ (corresponding to the intermediate eigenvector) are negative, while the cross correlations with $\cos(\omega, \boldsymbol{e}_1)$ and $\cos(\omega, \boldsymbol{e}_3)$ are always positive for both Couette and Poiseuille flows. This is in agreement with previous studies that showed that the probability of large value of $\cos(\omega, \boldsymbol{e}_2)$ is highest for any region.[72–74] Other studies also revealed that for near wall region, the value of relative helicity density is distributed around zero.[30,38,77] Therefore, when the vorticity aligns to the intermediate eigenvector, it tends to be perpendicular to the velocity vector.

The cross correlation for the absolute value of $\cos\theta'$ and $\cos(\boldsymbol{\omega}, \boldsymbol{e}_i)$ for the quartiles of the particles that disperse the least in the y direction and those that disperse the most at time $t = 100$ for release position at $Y_0 = 3$ are shown in Fig. 19. There is a remarkable difference between the data for the particles located closest and farthest away from the wall. The value of the cross correlation does not change a lot during the time of simulation for the particles moving closest, meanwhile the particles that disperse the most undergo a dramatic decrease in the value of the cross correlation coefficient to the value of zero. This can be explained by considering that the particles that are closer to the wall are those that are still located in the near wall region, being trapped in flow structures that are keeping them there. When they can escape these structures, then they can be transferred away from the wall by taking advantage of synergisms between different structures.[56] For the particles that are the farthest away from the wall, the cross correlation in these regions is nearly zero.

It has been found in Lagrangian tracking that the alignment between turbulence properties is affected by nonlocal structures

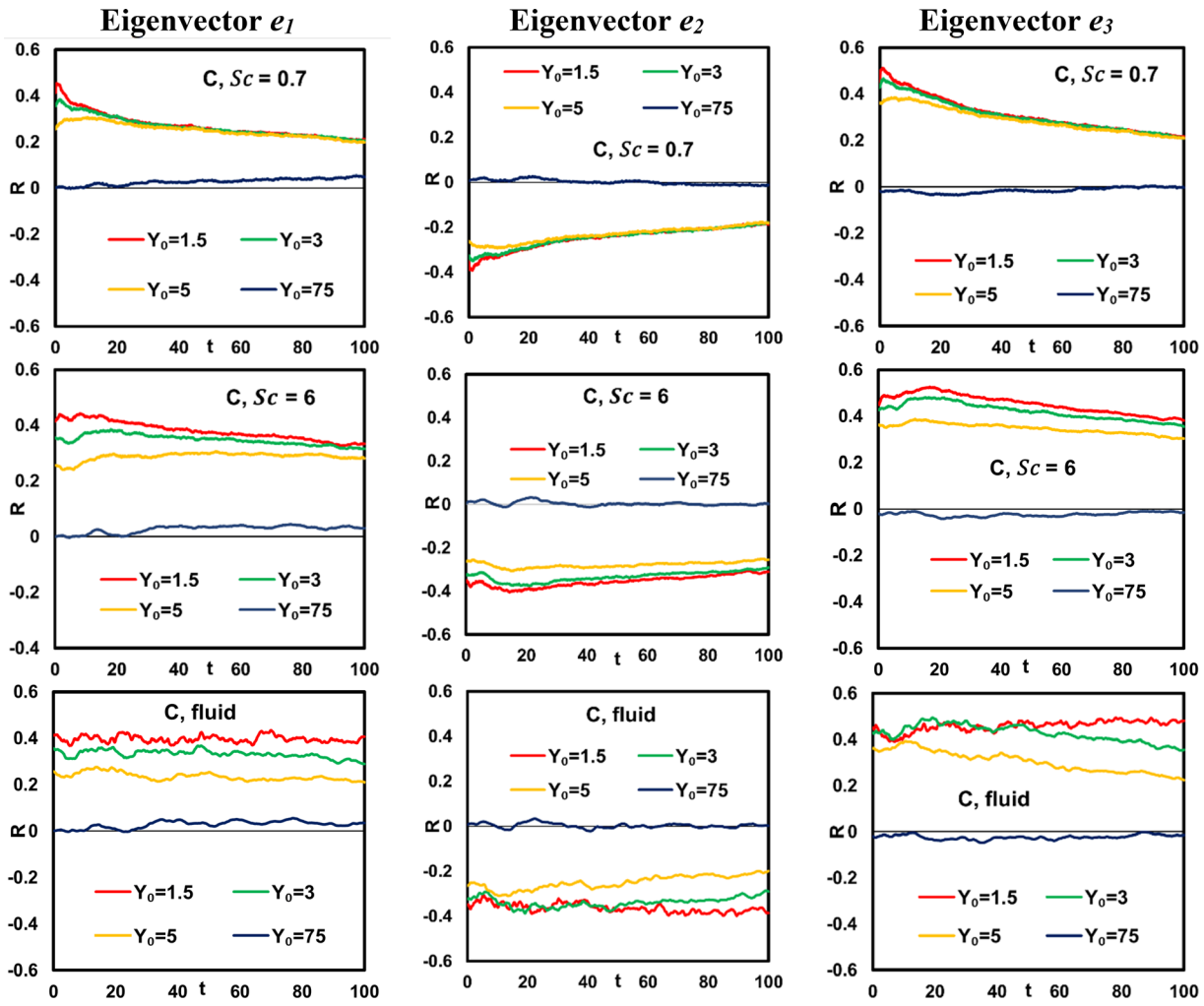

FIG. 18. Cross correlation between absolute value of relative helicity $h' = \cos\theta'$ and absolute value of the cosine between vorticity and the eigenvectors of the rate of strain tensor, $\cos(\omega, \mathbf{e}_i)$. $\mathbf{e}_i$ with $i = 1$–3 corresponds to eigenvectors with eigenvalues $\lambda_1 \geq \lambda_2 \geq \lambda_3$, for Couette flow and various *Sc* numbers. Rows correspond to different *Sc*, while columns correspond to different eigenvectors.

(see, for example, the pirouette effect in turbulent flows by Xu *et al.*[78] and Hamlington *et al.*[79]) In the present case, nonlocal effects that take time to develop are not ignore, since we use a DNS to obtain the flow field in which the scalar and fluid markers propagate. The Lagrangian timescale for the flow is much smaller than the duration of our computations. As reported in our prior publication,[2] the Lagrangian timescale for helicity is a function of the distance from the wall, and even though it is larger than the Lagrangian timescale for the fluctuating velocity, it is not larger than 30 viscous wall time units (even in the center of the channel, it does not go over 50 viscous time units). Therefore, the correlation and cross correlation data presented in the manuscript include nonlocal effects that may appear in the particle location as time advances.

IV. SUMMARY AND CONCLUSIONS

This study explored the relation between relative helicity density and the physical characteristics of turbulence in channel and Couette flow using Lagrangian methods applied to a DNS. The Lagrangian approach allowed an investigation of the relation between helicity density of flow structures and the transport of scalars in the flow. The joint probability density function between relative helicity and vertical fluctuating velocity shows that scalars in the near wall region exist in areas where both h' and v' have small values but farther from the wall the vertical velocity and the relative helicity density have larger values. This is reflected on the correlation of relative helicity density and normal velocity that directly affect transport of particles in the flow field. The JPDF for h' and v' provides evidence that the *Sc* and the location of particle release are more important than whether the flow is Poiseuille or Couette. The JPDFs between relative helicity and the orientation of the vorticity vector indicate that in the near wall region the vorticity vector is not aligned to the velocity vector. For particles released outside the buffer region, there appears to be no correlation between h' and the vorticity vector orientation.

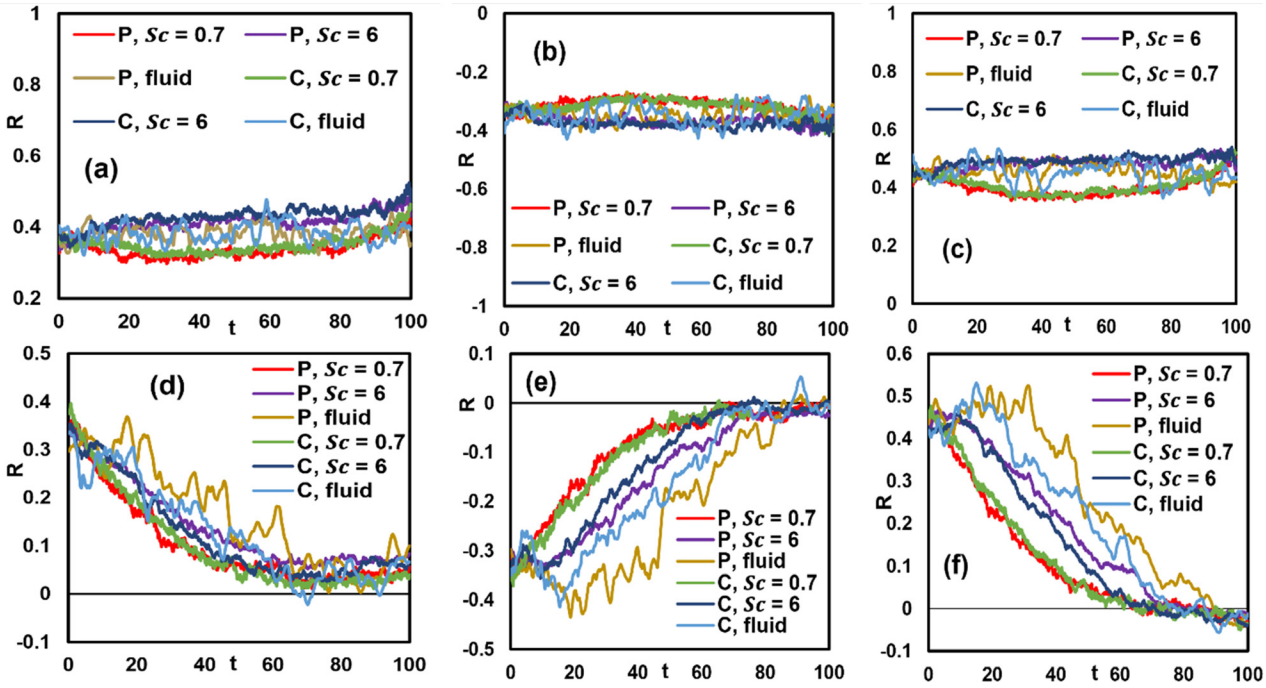

FIG. 19. Cross correlation between the absolute value of relative helicity $h' = \cos\theta'$ and absolute value of cosine between vorticity and eigenvectors $\cos(\omega, \mathbf{e}_i)$. $\mathbf{e}_i$ with i = 1–3 corresponds to eigenvectors of eigenvalues $\lambda_1 \geq \lambda_2 \geq \lambda_3$) for the10% of particles that are located closer for (a) $\mathbf{e}_1$, (b) $\mathbf{e}_2$, (c) $\mathbf{e}_3$ and farther (d) $\mathbf{e}_1$, (e) $\mathbf{e}_2$, and (f) $\mathbf{e}_3$ from the initial position $Y_0 = 3$ for Couette and Poiseuille flows at various *Sc* numbers.

The distribution of helicity conditioned on coherent structure identification indices, such as the Reynolds stress quadrants, the *Q*-criterion for vortex identification, and the second largest eigenvalue of the rate of strain tensor showed that the alignment between the vorticity and velocity vectors depends on the region of the flow from where the particles were released and on the effects of molecular diffusivity, expressed through the *Sc* number. The same conclusion can be drawn when considering the vector plot of instantaneous fluctuating velocity and the magnitude of relative helicity density for particles in both Poiseuille and Couette flows. In the near wall region, the relative helicity of particles has small values, meaning that the velocity and vorticity vectors are perpendicular to each other. Within the logarithmic layer region, the values of relative helicity were distributed in a range of broader values, extending in a more uniform fashion from −1 to 1. These distribution profiles are similar regardless of whether the distribution is conditioned on any criterion used herein for identifying coherent structures. This indicates that the vorticity and velocity vectors tend to align as particles move farther from the wall, in agreement with prior findings.[38]

The Lagrangian autocorrelation coefficient for *Q* values along particle trajectories was computed and the obtained results suggest that this autocorrelation coefficient is larger than zero for at least 100 viscous time units, while its values depend on *Sc*, the particle release position and the type of flow. When it comes to the relation between relative helicity and the alignment of vorticity with eigenvectors of the rate of strain tensor, it is found that the value of the relative helicity has an anti-correlation to the projection of vorticity on the intermediate eigenvectors of rate of strain tensor. There is a difference in the cross correlation between relative helicity density and the alignment of vorticity with the three eigenvectors of the rate of strain tensor at various *Sc* numbers, release position and the farthest and closest particles. The particles closest to the wall presented a higher correlation coefficient for longer times than particles that moved the farthest form the wall.

Separating the particles into those that disperse the farthest from the wall and those that disperse the least, differences are observed. This is one of the most important findings herein. The particles that disperse farther are those associated with sheet-like structures and those that do not appear to stay on one vortex longer. This is in agreement with prior results that argued for a major contribution to transport due to synergistic effects between flow structures. The physical picture is that those particles that disperse most are those that get away from the wall region because of a vortex, but then they are picked up by other eddies that enhance transport. The velocity and vorticity vectors along the trajectories of these particles may be perpendicular to each other initially but lose this characteristic at later times and farther from the wall.

SUPPLEMENTARY MATERIAL

See the supplementary material for complete data of different particle release positions. First, data for the JPDF between the relative helicity density h' and the fluctuating velocity in the direction normal to the channel wall, and then data for the JPDF between h' and α and for the PDF of h' conditioned on Reynolds stress quadrants. These data complement Figs. 1, 2, and 5–7.

ACKNOWLEDGMENTS

Financial support of the National Science Foundation (Grant No. CBET-1803014) is gratefully acknowledged, as is the use of

computing facilities at the University of Oklahoma Supercomputing Center for Education and Research (OSCER) and at XSEDE and ACCESS (under Allocation No. CTS-090025).

AUTHOR DECLARATIONS

Conflict of Interest

The authors have no conflicts to disclose.

Author Contributions

Oanh L. Pham: Conceptualization (equal); Data curation (lead); Formal analysis (equal); Investigation (equal); Methodology (equal); Software (lead); Validation (lead); Visualization (lead); Writing – original draft (equal); Writing – review & editing (equal). **Dimitrios V. Papavassiliou:** Conceptualization (equal); Formal analysis (equal); Funding acquisition (lead); Investigation (equal); Methodology (equal); Project administration (lead); Resources (lead); Supervision (lead); Writing – original draft (equal); Writing – review & editing (equal).

DATA AVAILABILITY

The data that support the findings of this study are available within the article and its supplementary material.

NOMENCLATURE

D	Molecular diffusivity
$d\overline{U}/dy$	The derivative of the mean velocity in the Eulerian framework
$\boldsymbol{e_i}$	The eigenvectors corresponding to eigenvalues λ_i of rate of strain tensor.
G	Constant for determining the channel wall velocity in place Couette flow
H	Helicity density $\mathbf{H} = \boldsymbol{u} \cdot \boldsymbol{\omega}$
H'	Helicity density for the fluctuating velocity, $\mathbf{H}' = \boldsymbol{u}' \cdot \boldsymbol{\omega}'$
$\mathcal{H}$	Total helicity
h	Half channel height
h′	Relative helicity density
PDF	Probability density function
Q	Q values computed based on Q-criterion as defined in Eq. (7)
Q1, Q2, Q3, and Q4	Turbulent events associated with each quadrant are called outward interactions (quadrant 1, Q1, $u' > 0$ and $v' > 0$), ejections (quadrant 2, Q2, $u' < 0$ and $v' > 0$), downward interactions (quadrant 3, Q3, $u' < 0$ and $v' < 0$), and sweeps (quadrant 4, Q4, $u' > 0$ and $v' < 0$).
Re	The Reynolds number
$R_{h'-\epsilon}$	The cross-correlation between relative helicity density h′ and $\epsilon_i = \cos(\omega, \boldsymbol{e}_i)$
$R_{Q-Q(t)}$	The Lagrangian autocorrelation coefficient for Q is calculated for particles released at different distances from the channel wall
Sc	The Schmidt number
S_{ij}	The local rate of strain tensor
t	Time
$\boldsymbol{U}$	The Eulerian velocity vector of the fluid at the location of the marker at time t
$\overline{U}$	The mean velocity
U_c	The mean centerline velocity of the channel
U_w	The streamwise velocity at the wall
$\mathbf{u}$	Velocity vector
$\boldsymbol{u}'$	The fluctuating velocity vector
u^*	The friction velocity
$\overline{u^2}$	the mean square of the x-component of the velocity of the fluid particles
u', v', and w'	Fluctuating velocity components in x, y, and z directions, respectively.
$\boldsymbol{X}_o$	The location that a marker was released at time t_0
$\boldsymbol{X}$	Position vector of a marker
X_f	The displacement of a fluid particle relative to its source
x, y, and z	The streamwise, normal and spanwise directions, respectively
$\boldsymbol{V}$	The Lagrangian velocity
Y_0	Distance from the bottom wall of the channel for particle release at time t_0 as viscous length scale
$\overline{Y}$	Average normal position of the markers

Greek symbols

α	The angle between vorticity vector and vertical direction
Δ	Change in quantity
ϵ	The turbulent dissipation rate along the trajectories of each marker
θ'	The angle between the fluctuating velocity and vorticity vectors
λ_i	The eigenvalues of strain rate tensor with the order $\lambda_1 \geq \lambda_2 \geq \lambda_3$
ν	The fluid kinematic viscosity
π	Trigonometric pi
σ	The standard deviation of the normal distribution that characterizes the random walk on the particle motion at the end of every convection step in viscous wall units
τ_{Ly}	Lagrangian timescale for dispersion in the direction normal to the channel walls
τ_w	The wall shear stress
$\boldsymbol{\omega}$	Vorticity vector
$\boldsymbol{\omega}'$	The vorticity vector for the fluctuating velocity
$\boldsymbol{\Omega}_{ij}$	The ij component of the vorticity tensor

Superscripts and subscripts

$\overline{()}$	Ensemble average
$()_0$	value of a quantity at initial time of interest
$()_w$	Value at the wall of the channel
$()_c$	Value at the center channel
$\lvert\,\rvert$	Absolute value
$\lVert\,\rVert$	The Euclidean (or Frobenius) matrix norm

REFERENCES

[1]O. G. Chkhetiani and E. Golbraikh, "Turbulent field helicity fluctuations and mean helicity appearance," Int. J. Non-Linear Mech. **47**, 113 (2012).

[2]O. L. Pham and D. V. Papavassiliou, "Helicity and dissipation correlation in anisotropic turbulent flow fields," Phys. Fluids **35**, 105135 (2023).
[3]Z. Yan, X. Li, J. Wang, and C. Yu, "Effect of pressure on joint cascade of kinetic energy and helicity in compressible helical turbulence," Phys. Rev. E **99**, 033114 (2019).
[4]A. Alexakis, "Helically decomposed turbulence," J. Fluid Mech. **812**, 752 (2017).
[5]M. A. Olshanskii and L. G. Rebholz, "Velocity–vorticity–helicity formulation and a solver for the Navier–Stokes equations," J. Comput. Phys. **229**, 4291 (2010).
[6]Z. Yan, X. Li, and C. Yu, "Scale locality of helicity cascade in physical space," Phys. Fluids **32**, 061705 (2020).
[7]H. K. Moffatt and A. Tsinober, "Helicity in laminar and turbulent flow," Annu. Rev. Fluid Mech. **24**, 281 (1992).
[8]Q. Chen, S. Chen, and G. L. Eyink, "The joint cascade of energy and helicity in three-dimensional turbulence," Phys. Fluids **15**, 361 (2003).
[9]Z. Yan, X. Li, C. Yu, J. Wang, and S. Chen, "Dual channels of helicity cascade in turbulent flows," J. Fluid Mech. **894**, R2 (2020).
[10]A. Povitsky, "Three-dimensional flow with elevated helicity in driven cavity by parallel walls moving in perpendicular directions," Phys. Fluids **29**, 083601 (2017).
[11]F. Capuano and D. Vallefuoco, "Effects of discrete energy and helicity conservation in numerical simulations of helical turbulence," Flow, Turbul. Combust. **101**, 343 (2018).
[12]R. B. Pelz, L. Shtilman, and A. Tsinober, "The helical nature of unforced turbulent flows," Phys. Fluids **29**, 3506 (1986).
[13]W. Polifke, "Statistics of helicity fluctuations in homogeneous turbulence," Phys. Fluids A **3**, 115 (1991).
[14]Y. Levy, A. Seginer, and D. Degani, "Graphical representation of three-dimensional vortical flows by means of helicity density and normalized helicity," in *Proceedings of 6th Applied Aerodynamics Conference* (AIAA, 1988).
[15]W. Agoua, B. Favier, and A. Delache, "Spontaneous generation and reversal of helicity in anisotropic turbulence," Phys. Rev. E **103**, L061101 (2021).
[16]H. K. Moffatt, "Transport effects associated with turbulence with particular attention to the influence of helicity," Rep. Prog. Phys. **46**, 621 (1983).
[17]J. C. Andre and M. Lesieur, "Influence of helicity on the evolution of isotropic turbulence at high Reynolds number," J. Fluid Mech. **81**, 187 (2006).
[18]R. H. Kraichnan, "Diffusion of passive-scalar and magnetic fields by helical turbulence," J. Fluid Mech. **77**(4), 753 (1976).
[19]C. Yu, R. Hu, Z. Yan, and X. Li, "Helicity distributions and transfer in turbulent channel flows with streamwise rotation," J. Fluid Mech. **940**, A18 (2022).
[20]L. Biferale, S. Musacchio, and F. Toschi, "Split energy–helicity cascades in three-dimensional homogeneous and isotropic turbulence," J. Fluid Mech. **730**, 309 (2013).
[21]N. Yokoi and A. Brandenburg, "Large-scale flow generation by inhomogeneous helicity," Phys. Rev. E **93**, 033125 (2016).
[22]Z. Yan, X. Li, and C. Yu, "Helicity budget in turbulent channel flows with streamwise rotation," Phys. Fluids **34**, 065105 (2022).
[23]K. Inagaki, N. Yokoi, and F. Hamba, "Mechanism of mean flow generation in rotating turbulence through inhomogeneous helicity," Phys. Rev. Fluids **2**, 114605 (2017).
[24]Y. Li, "Geometrical statistics and vortex structures in helical and nonhelical turbulences," Phys. Fluids **22**, 035101 (2010).
[25]U. Morbiducci, R. Ponzinib, M. Grigionid, and A. Redaelli, "Helical flow as fluid dynamic signature for atherogenesis risk in aortocoronary bypass. A numeric study," J. Biomech. **40**, 519 (2007).
[26]J. Jeong, F. Hussain, W. Schoppa, and J. Kim, "Coherent structures near the wall in a turbulent channel flow," J. Fluid Mech. **332**, 185 (1997).
[27]S. K. Robinson, "Coherent motions in the turbulent boundary layer," Annu. Rev. Fluid Mech. **23**, 601 (1991).
[28]J. Jiménez, "Coherent structures in wall-bounded turbulence," J. Fluid Mech. **842**, P1 (2018).
[29]L. Shtilman, R. B. Pelz, and A. Tsinober, "Numerical investigation of helicity in turbulent flow," Comput. Fluids **16**, 341 (1988).
[30]M. M. Rogers and P. Moin, "Helicity fluctuations in incompressible turbulent flows," Phys. Fluids **30**, 2662 (1987).
[31]Y. Zhang, K. Liu, H. Xian, and X. Du, "A review of methods for vortex identification in hydroturbines," Renewable Sustainable Energy Rev. **81**, 1269 (2018).
[32]J. M. Wallace, J. L. Balint, and L. Ong, "An experimental study of helicity density in turbulent flows," Phys. Fluids A **4**, 2013 (1992).
[33]A. Tsinober and E. Levich, "On the helical nature of three-dimensional coherent structures in turbulent flows," Phys. Lett. **99A**, 321 (1983).
[34]E. Levich and A. Tsinober, "On the role of helical structures in three-dimensional turbulent flow," Phys. Lett. **93A**, 293 (1982).
[35]R. B. Pelz, "Velocity-vorticity patterns in turbulent flow," Phys. Rev. Lett. **54**, 2505 (1985).
[36]L. Shtilman, S. E. Levich, A. Orszag, R. B. Pelz, and A. Tsinober, "On the role of helicity in complex fluid flows," Phys. Lett. **113A**, 32 (1985).
[37]C. G. Speziale, "On helicity fluctuations in turbulence," Q. Appl. Math. **45**, 123 (1987).
[38]Q. Nguyen and D. V. Papavassiliou, "Using helicity to investigate scalar transport in wall turbulence," Phys. Rev. Fluids **5**, 062601 (2020).
[39]D. V. Papavassiliou, "Turbulent transport from continuous sources at the wall of a channel," Int. J. Heat Mass Transfer **45**, 3571 (2002).
[40]B. Debusschere and C. J. Rutland, "Turbulent scalar transport mechanisms in plane channel and Couette flows," Int. J. Heat Mass Transfer **47**, 1771 (2004).
[41]S. L. Lyons, T. J. Hanratty, and J. B. McLaughlin, "Large-scale computer simulation of fully developed turbulent channel flow with heat transfer," Numer. Methods Fluids **13**, 999 (1991).
[42]S. A. Orszag, "On the elimination of aliasing in finite-difference schemes by filtering high-wavenumber components," J. Atmos. Sci. **28**, 1074 (1971).
[43]A. Günther, D. V. Papavassiliou, M. D. Warholic, and T. J. Hanratty, "Turbulent flow in a channel at a low Reynolds number," Exp. Fluids **25**, 503 (1998).
[44]S. L. Lyons, "A direct numerical simulation of fully developed turbulent channel flow with passive heat transfer," Ph.D. dissertation (University of Illinois, 1989).
[45]B. M. Mitrovic and D. V. Papavassiliou, "Effects of a first-order chemical reaction on turbulent mass transfer," Int. J. Heat Mass Transfer **47**, 43 (2004).
[46]O. L. Pham, S. E. Feher, Q. T. Nguyen, and D. V. Papavassiliou, "Computations of the shear stresses distribution experienced by passive particles as they circulate in turbulent flow: A case study for vWF protein molecules," PLoS One **17**, e0273312 (2022).
[47]D. V. Papavassiliou and T. J. Hanratty, "Transport of a passive scalar in a turbulent channel flow," Int. J. Heat Mass Transfer **40**, 1303 (1997).
[48]D. V. Papavassiliou and T. J. Hanratty, "The use of Lagrangian methods to describe turbulent transport of heat from a wall," Ind. Eng. Chem. Res. **34**, 3359 (1995).
[49]C. Srinivasan and D. V. Papavassiliou, "Direction of scalar transport in turbulent channel flow," Phys. Fluids **23**, 115105 (2011).
[50]D. V. Papavassiliou, "Scalar dispersion from an instantaneous line source at the wall of a turbulent channel for medium and high Prandtl number fluids," Int. J. Heat Fluid Flow **23**, 161 (2002).
[51]K. Kontomaris, T. J. Hanratty, and J. B. McLaughlin, "An algorithm for tracking fluid particles in a spectral simulation of turbulent channel flow," J. Comput. Phys. **103**, 231 (1992).
[52]O. L. Pham, S. E. Feher, Q. T. Nguyen, and D. V. Papavassiliou, "Distribution and history of extensional stresses on vWF surrogate molecules in turbulent flow," Sci. Rep. **12**, 171 (2022).
[53]Q. Nguyen and D. V. Papavassiliou, "Scalar mixing in anisotropic turbulent flow," AIChE J. **64**, 2803 (2018).
[54]Q. Nguyen and D. V. Papavassiliou, "A statistical model to predict streamwise turbulent dispersion from the wall at small times," Phys. Fluids **28**, 125103 (2016).
[55]P. M. Le and D. V. Papavassiliou, "A physical picture of the mechanism of turbulent heat transfer from the wall," Int. J. Heat Mass Transfer **52**, 4873 (2009).
[56]A. K. Karna and D. V. Papavassiliou, "Near-wall velocity structures that drive turbulent transport from a line source at the wall," Phys. Fluids **24**, 035102 (2012).
[57]E. R. Corino and R. S. Brodkey, "A visual investigation of the wall region in turbulent flow," J. Fluid Mech. **37**, 1 (2006).
[58]S. G. Nychas, H. C. Hershey, and R. S. Brodkey, "A visual study of turbulent shear flow," J. Fluid Mech. **61**, 513 (2006).

[59]J. H. A. Hogenes and T. J. Hanratty, "The use of multiple wall probes to identify coherent flow patterns in the viscous wall region," J. Fluid Mech. **124**, 363 (2006).
[60]M. K. Lee, L. D. Eckelman, and T. J. Hanratty, "Identification of turbulent wall eddies through the phase relation of the components of the fluctuating velocity gradient," J. Fluid Mech. **66**, 17 (2006).
[61]C. D. Dritselis and N. S. Vlachos, "Numerical investigation of momentum exchange between particles and coherent structures in low Re turbulent channel flow," Phys. Fluids **23**, 025103 (2011).
[62]C. Srinivasan and D. V. Papavassiliou, "Comparison of backwards and forwards scalar relative dispersion in turbulent shear flow," Int. J. Heat Mass Transfer **55**, 5650 (2012).
[63]D. Barkley and L. S. Tuckerman, "Mean flow of turbulent–laminar patterns in plane Couette flow," J. Fluid Mech. **576**, 109 (2007).
[64]D. V. Papavassiliou and T. J. Hanratty, "Interpretation of large-scale structures observed in a turbulent plane Couette flow," Int. J. Heat Fluid Flow **18**, 55 (1997).
[65]I. Vinkovic, D. Doppler, J. Lelouvetel, and M. Buffat, "Direct numerical simulation of particle interaction with ejections in turbulent channel flows," Int. J. Multiphase Flow **37**, 187 (2011).
[66]C. J. Kähler, "Investigation of the spatio-temporal flow structure in the buffer region of a turbulent boundary layer by means of multiplane stereo PIV," Exp. Fluids **36**, 114 (2003).
[67]Y. Huang, M. Rockwood, and M. A. Green, "Tracking coherent structures in massively-separated and turbulent flows," in *Ninth International Symposium on Turbulence and Shear Flow Phenomena (TSFP-9) 3D-2* (Begell House Inc., 2015).
[68]J. Jeong and F. Hussain, "On the identification of a vortex," J. Fluid Mech. **285**, 69 (2006).
[69]C. Srinivasan and D. V. Papavassiliou, "Backwards and forwards dispersion of a scalar in turbulent wall flows," Int. J. Heat Mass Transfer **53**, 1023 (2010).
[70]S. Zhang and D. Choudhury, "Eigen helicity density: A new vortex identification scheme and its application in accelerated inhomogeneous flows," Phys. Fluids **18**, 058104 (2006).
[71]R. M. Kerr, "Histograms of helicity and strain in numerical turbulence," Phys. Rev. Lett. **59**, 783 (1987).
[72]W. T. Ashurst, A. R. Kerstein, R. M. Kerr, and C. H. Gibson, "Alignment of vorticity and scalar gradient with strain rate in simulated Navier–Stokes turbulence," Phys. Fluids **30**, 2343 (1987).
[73]R. Gomes-Fernandes, B. Ganapathisubramani, and J. C. Vassilicos, "Evolution of the velocity-gradient tensor in a spatially developing turbulent flow," J. Fluid Mech. **756**, 252 (2014).
[74]K. Nakamura, T. Matsushima, Y. Zheng, K. Nagata, and T. Watanabe, "Large- and small-scale characteristics in a temporally developing shearless turbulent mixing layer," Phys. Fluids **34**, 115117 (2022).
[75]M. Danish and C. Meneveau, "Multiscale analysis of the invariants of the velocity gradient tensor in isotropic turbulence," Phys. Rev. Fluids **3**, 044604 (2018).
[76]Z. Liu, R. J. Adrian, and T. J. Hanratty, "Large-scale modes of turbulent channel flow: Transport and structure," J. Fluid Mech. **448**, 53 (2001).
[77]J. M. Wallace and J. L. Balint, "An experimental study of helicity and related properties in turbulent flows," in paper presented at the 1UTAM Symposium: Topological Fluid Mechanics, Cambridge, England, 1989.
[78]H. Xu, A. Pumir, and E. Bodenschatz, "The pirouette effect in turbulent flows," Nat. Phys. **7**, 709 (2011).
[79]P. E. Hamlington, J. Schumacher, and W. J. Dahm, "Local and nonlocal strain rate fields and vorticity alignment in turbulent flows," Phys. Rev. E **77**, 026303 (2008).